

The Sixteen $\text{CB}_{11}\text{H}_n\text{Me}_{12-n}^-$ Anions with Fivefold Substitution Symmetry: Anodic Oxidation and Electronic Structure

Benjamin T. King,^{†,‡} Stefanie Körbe,^{†,§} Peter J. Schreiber,[†] Joshua Clayton,[†] Adriana Němcová,[§] Zdeněk Havlas,[§] Kamesh Vyakaranam,[†] Matthew G. Fete,[†] Ilya Zharov,^{†,||} Jason Ceremuga,[†] and Josef Michl^{*,†,§}

Contribution from the Department of Chemistry and Biochemistry, University of Colorado, Boulder, Colorado 80309-0215, Institute of Organic Chemistry and Biochemistry, Academy of Sciences of the Czech Republic, 166 10 Prague 6, Czech Republic, and the Department of Chemistry, University of Nevada, Reno, Nevada 89557

Received September 12, 2006; Revised Manuscript Received May 11, 2007; E-mail: michl@eefus.colorado.edu

Abstract: The 15 symmetrically methylated derivatives of the $\text{CB}_{11}\text{H}_{12}^-$ anion (**1a**) have been synthesized and found to vary greatly in ease of oxidation. Cyclic voltammetry in liquid SO_2 yielded fully reversible oxidation potentials for five of those that have no adjacent unsubstituted vertices in positions 7–12; three others showed some indication of reversibility. The anions **1a–16a** and the Jahn–Teller distorted neutral radicals **1r–16r** have been characterized by ab initio and density functional theory calculations. In the state average CASSCF(13,12)/6-31+G* approximation, the ground state potential energy surface of **1r** contains five symmetry-related pairs of minima. The computational results account for the reversible redox potentials very well when the solvent is included explicitly (RI-DFT(BP)/TZVP, COSMO). For display and for a semiquantitative understanding of methyl substituent effects in terms of perturbation theory, the molecular orbitals of **1a** have been expressed in the symmetry-adapted cluster basis. The results serve as an underpinning for a set of additive empirical increments for redox potential prediction. Relative to the usual hydrogen standard, a single methyl group facilitates oxidation by approximately 50, 70, 70, and 10 mV in positions 1, 2, 7, and 12, respectively. This electron donor effect on the redox potential is due to a π contribution, whereas those of σ (inductive and direct field) type are negligible.

Introduction

In recent years, considerable attention has been paid to the $\text{CB}_{11}\text{H}_{12}^-$ anion¹ (**1a**, Chart 1). A recent review² reveals that much of it focused on the exploitation of the weakly coordinating nature^{3–5} of this anion and its derivatives. In attempts to optimize its properties, **1a** has been substituted, mostly with halogens, and the resulting anions have been used to prepare salts of unusual cations, often not accessible in any other known way.² Another remarkable feature is the highly lipophilic nature of polyalkylated derivatives of **1a**, which have a striking solubilizing ability for large organic⁶ and “naked” alkali metal⁷ cations in solvents of low polarity. In such solvents, naked lithium cations are potent Lewis acids. They strongly catalyze

pericyclic reactions⁸ and the radical-induced polymerization of terminal alkenes such as isobutylene.⁹ The focus of the present article lies on neither of these two main themes but on devising methods for selective substitution on **1a** and probing its electronic structure by examining the effects of methyl substitution on the ease of oxidation.

In addition to the parent **1a** ($n = 0$), there are a total of 15 anions $\text{CB}_{11}\text{H}_{12-n}\text{Me}_n^-$ **2a–16a** in which the methyl substitution pattern preserves the fivefold symmetry of the parent (Chart 1; for vertex numbering, see **16**). Some of these anions have not been reported previously. Most of those already known have only been described in dissertations,^{10–12} and **2a** and **16a**, also in a short communication.¹³ Only the preparations of **5a**,¹⁴ **8a**,¹⁴ and **12a**^{15,16} have been reported in full papers. We now provide

[†] University of Colorado.

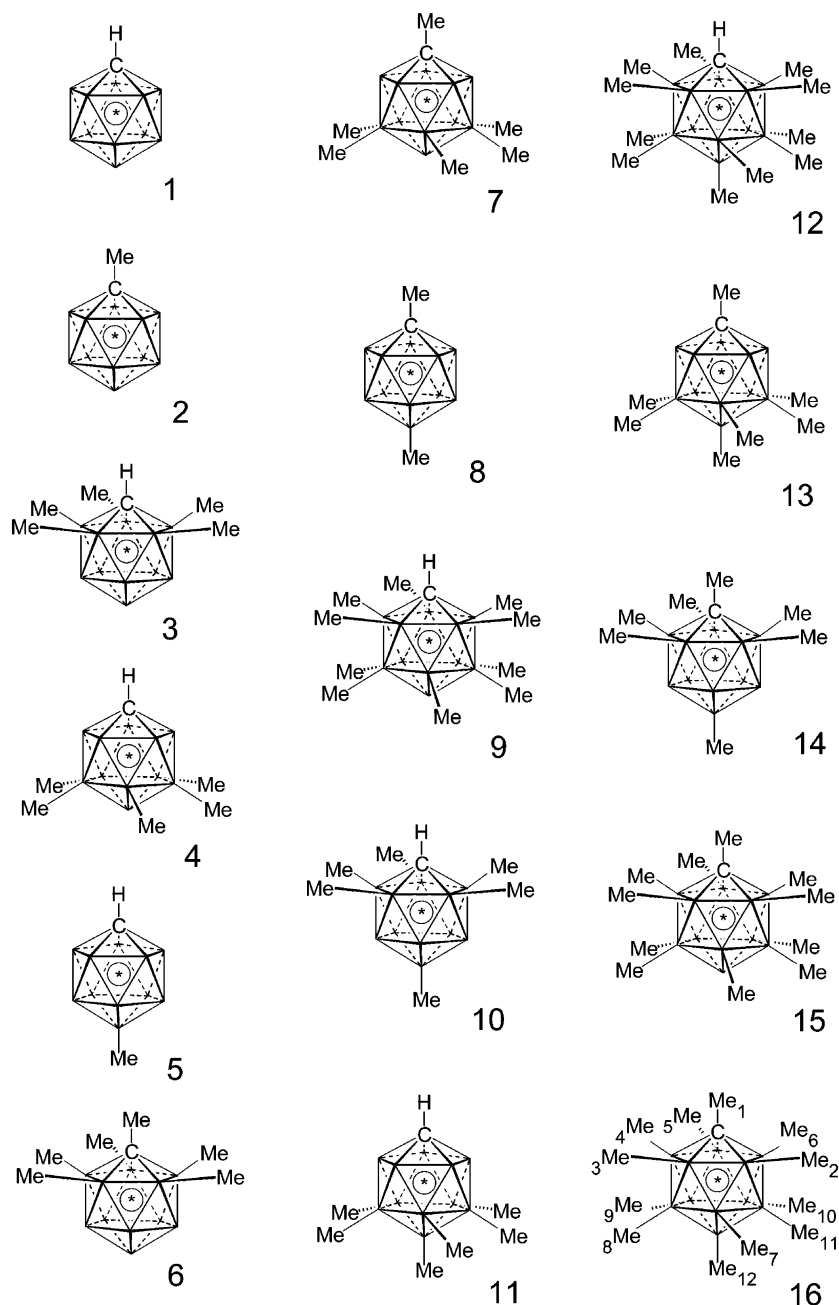
[‡] University of Nevada.

[§] Academy of Sciences of the Czech Republic.

^{||} Present address: Department of Chemistry, University of Utah, Salt Lake City, UT 84112-0850.

- (1) (a) Knoth, W. H. *J. Am. Chem. Soc.* **1967**, *89*, 1274. (b) Knoth, W. H. *Inorg. Chem.* **1971**, *10*, 598.
- (2) Körbe, S.; Schreiber, P. J.; Michl, J. *Chem. Rev.* **2006**, *106*, 5208.
- (3) (a) Plešek, J. *Chem. Rev.* **1992**, *92*, 269. (b) Stibr, B. *Chem. Rev.* **1992**, *92*, 225. (c) Krossing, I.; Raabe, I. *Angew. Chem., Int. Ed.* **2004**, *43*, 2066.
- (4) Strauss, S. H. *Chem. Rev.* **1993**, *93*, 927.
- (5) Strauss, S. H. In *Contemporary Boron Chemistry*; Wade, K.; Marder, T. B.; Hughes, A., Eds.; Royal Society of Chemistry: 2000; Vol. 253, p 44.
- (6) Valášek, M.; Pecka, J.; Jindřich, J.; Calleja, G.; Craig, P. R.; Michl, J. *J. Org. Chem.* **2005**, *70*, 405.
- (7) Pospíšil, L.; King, B. T.; Michl, J. *Electrochim. Acta* **1998**, *44*, 103.

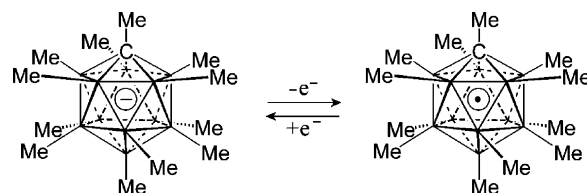
- (8) Moss, S.; King, B. T.; de Meijere, A.; Kozhushkov, S. I.; Eaton, P. E.; Michl, J. *Org. Lett.* **2001**, *3*, 2375.
- (9) Vyakaranam, K.; Barbour, J. B.; Michl, J. *J. Am. Chem. Soc.* **2006**, *128*, 5610.
- (10) Clayton, J. R. M.S. Thesis, University of Colorado, Boulder, CO, 1999.
- (11) King, B. T. Ph.D. Dissertation, University of Colorado, Boulder, CO, 2000.
- (12) Zharov, I. Ph.D. Dissertation, University of Colorado, Boulder, CO, 2000.
- (13) King, B. T.; Janoušek, Z.; Grüner, B.; Trammell, M.; Noll, B. C.; Michl, J. *J. Am. Chem. Soc.* **1996**, *118*, 3313.
- (14) Grüner, B.; Janoušek, Z.; King, B. T.; Woodford, J. N.; Wang, C. H.; Vřetečka, V.; Michl, J. *J. Am. Chem. Soc.* **1999**, *121*, 3122.
- (15) Tsang, C. W.; Yang, Q.; Sze, E. T.-P.; Mak, T. C. W.; Chan, D. T. W.; Xie, Z. *Inorg. Chem.* **2000**, *39*, 3582.
- (16) Clarke, A. J.; Ingleson, M. J.; Kociok-Köhn, G.; Mahon, M. F.; Patmore, N. J.; Rourke, J. P.; Ruggiero, G. D.; Weller, A. S. *J. Am. Chem. Soc.* **2004**, *126*, 1503.

Chart 1. Isomers of CB₁₁H_{12-n}Me_n^{*} with C_{5v} Substitution Pattern (Anions a, * = -; Radicals r, * = •)^a

^a Unsubstituted vertices represent BH, and substituted vertices represent B; the C vertex is shown explicitly. Vertex numbering is shown on **16**.

complete details for the preparation of all 15 symmetrically methylated anions derived from **1a**.¹⁷ We also describe a few additional anions containing other alkyl groups, which now join the 1-ethyl,¹⁸ many other 1-alkyl and 1-alkylundecamethyl,^{19,20} 4,6,8,10,12- pentaethyl,²¹ 1-H-undecaethyl,¹⁵ and several 12-alkyl¹⁴ derivatives of **1a** that are already known.

In acetonitrile, the parent **1a** is too hard to oxidize and yields no anodic wave,²² whereas **16a** shows a reversible peak¹³

Scheme 1. Reversible Redox Behavior of **16**

(Scheme 1). Relative to ferrocene/ferricenium (Fc/Fc⁺), the redox potential of **16a** lies at 1.16 V, and this can be compared with 0.56 V²³ for BPh₄⁻ and 2.1 V⁴ for B(C₆F₅)₄⁻. It was of interest to find out how the methyl groups in the four distinct

(17) Some of the results were mentioned in a brief review article: King, B. T.; Zharov, I.; Michl, J. *Chem. Innov.* **2001**, *31*, 23.

(18) Jelínek, T.; Baldwin, P.; Scheidt, W. R.; Reed, C. A. *Inorg. Chem.* **1993**, *32*, 1982.

(19) Vyakaranam, K.; Körbe, S.; Divišová, H.; Michl, J. *J. Am. Chem. Soc.* **2004**, *126*, 15795.

(20) Vyakaranam, K.; Körbe, S.; Michl, J. *J. Am. Chem. Soc.* **2006**, *128*, 5680.

(21) Molinos, E.; Kociok-Köhn, G.; Weller, A. S. *Chem. Commun.* **2005**, 3609.

(22) Wiersema, R. J.; Hawthorne, M. R. *Inorg. Chem.* **1973**, *12*, 785.

(23) Bancroft, E. E.; Blount, H. N.; Janzen, E. G. *J. Am. Chem. Soc.* **1979**, *1010*, 3692.

types of position contribute to the large decrease in the redox potential of **1a** upon substitution, and we have therefore examined the one-electron oxidation of the anions **1a–16a** to the corresponding radicals **1r–16r** by cyclic voltammetry in liquid SO₂.

In order to interpret the substituent effects in terms of molecular orbital (MO) theory at an intuitive level, the MOs of **1a** and its congeners obtained by ab initio and density functional theory (DFT) calculations for **1a–16a** are best expressed in terms of the easily visualized symmetry-adapted cluster basis set. This facilitates the use of perturbation theory to evaluate the electronic effect of a methyl group on a boron cluster framework, which has been of recent interest.²⁴ However, comparison with the observed redox potentials need not be straightforward, because the highest molecular orbital (HOMO) of **1a** is degenerate and the ground state of the radical **1r** is subject to Jahn–Teller distortion.²⁵

The oxidation of **16a** has also been carried out chemically, and the neutral radical **16r** has been isolated.²⁶ Its stability is attributable to a combination of steric hindrance to dimerization and lower redox potential. The present electrochemical results suggest that four additional radicals of the series are likely to be similarly stable and indicate that a new family of lipophilic reversible one-electron oxidizing agents with graded power is within reach.

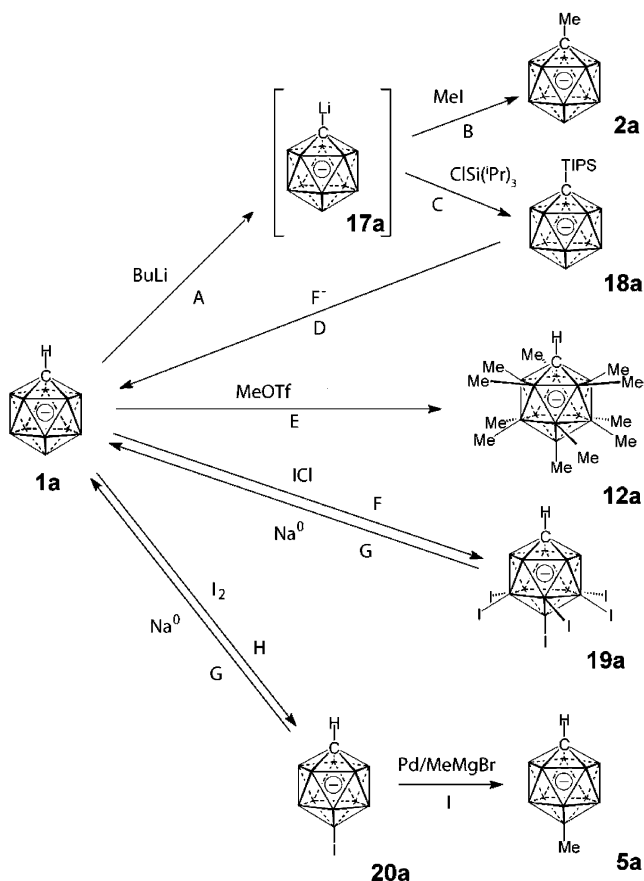
The radical **16r** has already proven useful as an oxidant soluble in nonpolar solvents, because the byproduct **16a** to which it is converted is a weak nucleophile, not likely to interfere excessively in syntheses of reactive cations.^{27,28} Another possible use of peralkylated derivatives of **1r** is in the preparation of redox polymers and molecular wires, where the ability to tune the redox potential by a choice of methyl substitution patterns would be especially desirable. The synthesis¹⁹ and Li⁺-catalyzed radical polymerization²⁰ of the appropriate permethylated monomers, derivatives of **12a** with a terminal 1-alkenyl substituent, have already been accomplished, as has the coupling of two anions **12a** through ethene and ethyne bridges.²⁹

In another recent development, **16r** has been used as a methyl radical donor and a source of an electroneutral hypercloso CB₁₁ cluster with a naked boron vertex.³⁰

Results and Discussion

Synthesis of Methylated Anions. Methods. To achieve selective methylation, we have relied on three different procedures for methyl group introduction and have taken advantage of the known^{31,32} different reactivities of nonequivalent BH vertices toward electrophilic substitution (fastest in position 12, slower in 7–11, and slowest in 2–6). We have also exploited

Scheme 2. Synthetic Tools for Regioselective Derivatization of **1a**



the effect of iodination on the acidity of the carbon vertex and have devised two blocking/unblocking strategies.

The synthetic tools used are summarized in Scheme 2, which also shows the structures of synthetic intermediates **17a–20a**. The first alkylation method is the selective deprotonation–metalation of the CH vertex with *n*-butyllithium or *tert*-butyllithium followed by electrophilic substitution with an alkyl halide or tosylate (reactions A and B). This process had precedent in both neutral³³ and anionic^{18,31} 12-vertex carboranes. The acidity of the CH vertex in **1a** is very sensitive to substituent effects,³⁴ and **4a**, **11a**, and **12a** are not deprotonated by *n*-BuLi, *tert*-BuLi, or *n*-BuMg–*N*-*i*-Pr₂.³⁵ However, after the introduction of a sufficient number of iodine substituents to some of the positions 2–11, **4a** and **11a** can be deprotonated.

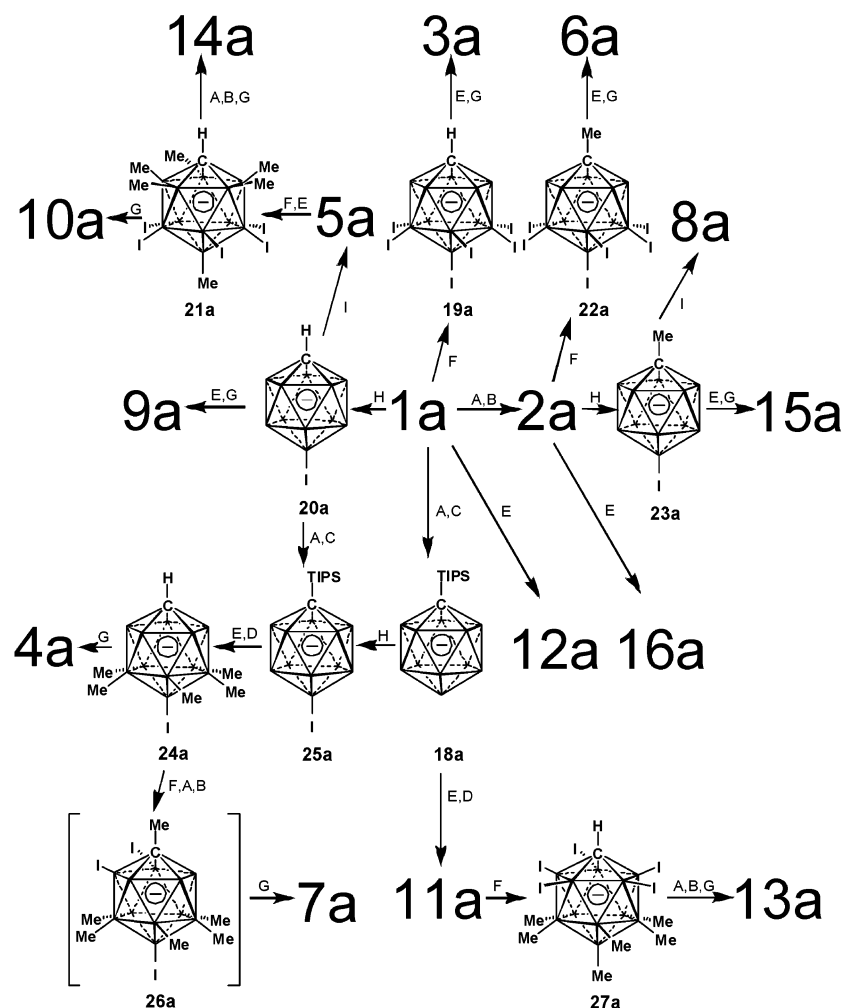
The second alkylation method is the palladium-catalyzed Kumada coupling of a Grignard reagent with an iodinated boron vertex (reaction I), which was also preceded in both neutral^{36–38} and anionic¹⁴ carboranes. It proceeds well but tends to give low yields when many iodine atoms are to be replaced simultaneously.

The third alkylation method is electrophilic methylation of BH vertices with methyl triflate (reaction E), usually in the presence of a base to neutralize the triflic acid generated in the

- (24) Teixidor, F.; Barberà, G.; Vaca, A.; Kivekäs, R.; Sillanpää, R.; Oliva, J.; Viñas, C. *J. Am. Chem. Soc.* **2005**, *127*, 10158.
 (25) McKee, M. *J. Am. Chem. Soc.* **1997**, *119*, 4220.
 (26) King, B. T.; Noll, B. C.; McKinley, A. J.; Michl, J. *J. Am. Chem. Soc.* **1996**, *118*, 10902.
 (27) Zharov, I.; King, B. T.; Havlas, Z.; Pardi, A.; Michl, J. *J. Am. Chem. Soc.* **2000**, *122*, 10253.
 (28) Zharov, I.; Weng, T.; Orendt, A. M.; Barich, D. H.; Penner-Hahn, J.; Grant, D. M.; Havlas, Z.; Michl, J. *J. Am. Chem. Soc.* **2004**, *126*, 12033.
 (29) Eriksson, L.; Vyakaranam, K.; Ludvík, J.; Michl, J. *J. Org. Chem.* **2007**, *72*, 2351.
 (30) Zharov, I.; Havlas, Z.; Orendt, A. M.; Barich, D. H.; Grant, D. M.; Fete, M. G.; Michl, J. *J. Am. Chem. Soc.* **2006**, *128*, 6089.
 (31) Jelínek, T.; Plešek, J.; Heřmánek, S.; Štíbr, B. *Coll. Czech. Chem. Commun.* **1986**, *51*, 819.
 (32) Jelínek, T.; Plešek, J.; Mareš, F.; Heřmánek, S.; Štíbr, B. *Polyhedron* **1987**, *6*, 1981.

- (33) Bregadze, V. I. *Chem. Rev.* **1992**, *92*, 209.
 (34) Schreiber, P. J. Ph.D. Dissertation, University of Colorado, Boulder, CO, 2007.
 (35) Zhang, M.; Eaton, P. E. *Angew. Chem., Int. Ed.* **2002**, *41*, 2169.
 (36) Zakharkin, L. I.; Kovredov, A. I.; Ol'shevskaya, V. A.; Shaugumbekova, Zh. S. *J. Organomet. Chem.* **1982**, *226*, 217.
 (37) Li, J.; Logan, C. F.; Jones, M., Jr. *Inorg. Chem.* **1991**, *30*, 4866.
 (38) Zheng, Z.; Jiang, W.; Zinn, A. A.; Knobler, C. B.; Hawthorne, M. F. *Inorg. Chem.* **1995**, *34*, 2095.

Scheme 3. Syntheses of 2a–16a Starting from 1a



reaction.¹³ Initially, 2,6-di-*tert*-butylpyridine and CaH₂ were used, but an improved procedure which uses sulfolane as the solvent and only CaH₂ as the base has been developed.³⁹ The reaction is similar to the concurrently developed analogous methylation of neutral carboranes,⁴⁰ which requires catalysis by a strong acid.

Methylation of BH vertices with methyl triflate is usually synthetically useful only if all free vertices present are to be substituted, since otherwise it is apt to produce complex mixtures. Only on rare occasions is the reactivity of nonequivalent vertices differentiated sufficiently for some of them to remain unmethylated in good yield.⁴¹ We find that boron methylation can be made selective for positions 7–12 if the bulky triisopropylsilyl (TIPS) group is placed on the carbon vertex (reactions A and C). The TIPS group is easily removable with warm water before the methylation but is much harder to remove afterward, in line with the low acidity of the methylated anions (reaction D). The best choice is wet tetrabutylammonium fluoride (TBAF) in DMF at 80 °C. This is an improvement over the previously used¹¹ heating with the Schwesinger fluoride⁴² to 180 °C or with CsF to 280 °C.

A second useful blocking substituent that we have found is iodine, which prevents methylation in the ipso position. It is not foolproof, in that in triflic acid iodine is known⁴³ to be replaceable with chlorine, and we have observed rare instances in which methyl triflate replaced an iodine substituent with a methyl, too. However, the blocking works well in the cases described in the present paper. Iodine can be introduced selectively at position 12³¹ (reaction H) or at all six positions 7–12⁴⁴ (reaction F). When the positions 7–12 are blocked, iodine enters into positions 2–6, often with some difficulty.

Iodination with one (reaction H) or several (reaction F) iodines has served three purposes. It blocks a boron vertex from electrophilic substitution, it activates the vertex for Pd-catalyzed coupling, and in positions 2–11, it enhances the acidity of the CH vertex. In the first and the third case the iodine needs to be removed after it has served its purpose. This is accomplished by reduction under Birch conditions (reaction G). The reduction is best performed by addition of a solution of the iodinated anion to a solution of excess sodium metal and some alcohol in liquid ammonia. The inverse addition of sodium to a solution of the iodinated anion in liquid ammonia causes the formation of

(39) Clayton, J. R.; King, B. T.; Zharov, I.; Fete, M. G.; Michl, J. submitted for publication.

(40) Jiang, W.; Knobler, C. B.; Mortimer, M. D.; Hawthorne, M. F. *Angew. Chem., Int. Ed.* **1995**, *34*, 1332.

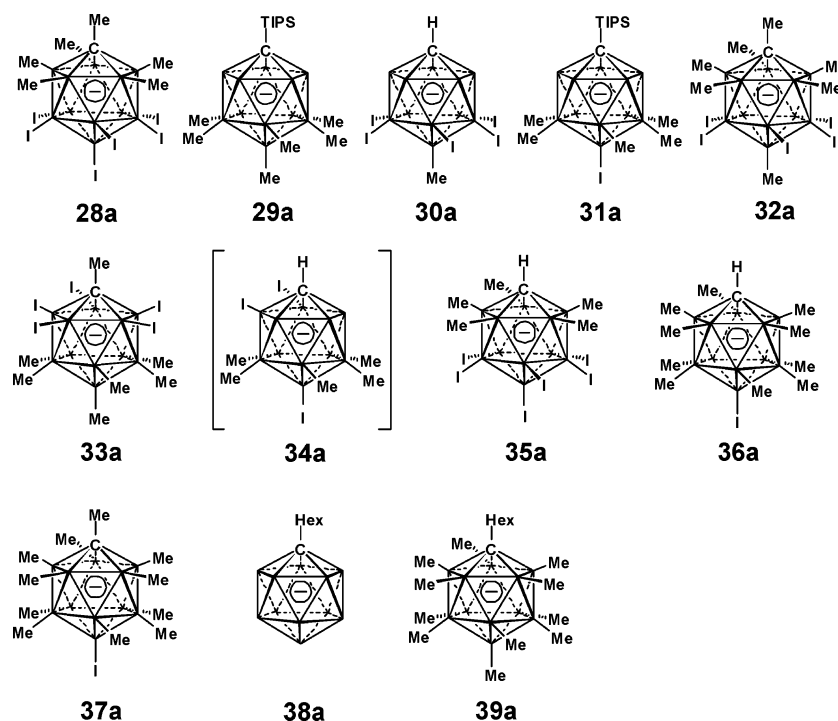
(41) Vyakaranam, K.; Janoušek, Z.; Eriksson, L.; Michl, J. *Heteroatom Chem.* **2006**, *17*, 217.

(42) Schwesinger, R.; Link, R.; Thiele, G.; Rotter, H.; Honert, D.; Limbach, H. H.; Mannle, R. *Angew. Chem., Ed. Engl.* **1991**, *30*, 1372.

(43) Xie, Z.; Tsang, C.; Sze, E. T.; Yang, Q.; Chan, D. T. W.; Mak, T. C. W. *Inorg. Chem.* **1998**, *37*, 6444.

(44) Xie, Z.; Manning, J.; Reed, R. W.; Mathur, R.; Boyd, P. D. W.; Benesi, A.; Reed, C. A. *J. Am. Chem. Soc.* **1996**, *118*, 2922.

Chart 2. Anion Structures



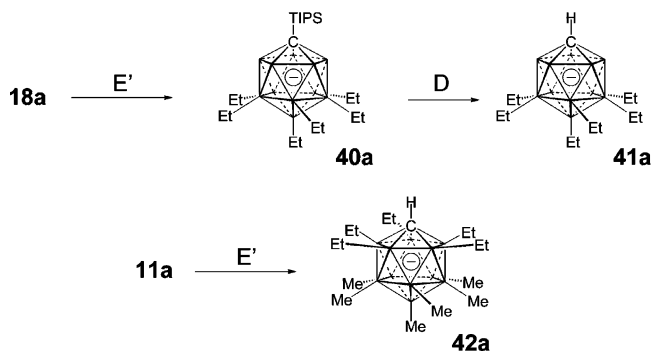
byproducts carrying scrambled numbers of methyl substituents on the carborate anion, with one methylated cage apparently serving as a methylating agent for another. This peculiar process has not yet been investigated in detail.

Selective Methylation Paths. Scheme 2 has already illustrated the formation of **2a**, **5a**, and **12a**, using the three modes of methylation, and presented the structures of intermediates **17a–20a**. Scheme 3 summarizes the paths taken from **1a** to all 15 anions **2a–16a** via the additional intermediates **21a–27a**. The structures of intermediates **28a–39a**, not shown explicitly in Scheme 3, are collected in Chart 2.

Scheme 3 requires only two brief comments. A pentamethylation reaction on the path to **4** and **7** required a reversed-phase chromatographic separation of the product from impurities due to overmethylation and undermethylation. Whereas the blocking effect of the TIPS group in **18a** is perfect and exhaustive methylation yields only the hexamethylated product, an iodine in position 12 reduces the reactivity difference between positions 2–6 and 7–11, apparently by activating the former and deactivating the latter. Deactivation of adjacent positions in methylation with methyl triflate has also been noted with an iodine in position 1.⁴¹ Under the conditions used for **18a**, and even at 0 °C, some overmethylation occurred with **25a**. At shorter times, some incompletely methylated product remained while an overmethylated product was already formed.

The iodination of **4a**, needed to render its carbon vertex sufficiently acidic for methylation on the way to **7a**, is relatively difficult, and we were unable to pentaiodinate in positions 2–6 in good yield. However, already partial iodination to a mixture **34a**, in which the diiodo anion dominated, turned out to be sufficient. The mixture was deprotonated and methylated and then reduced to afford **7a**.

In an attempt to permit future investigations of salts that are even more soluble in nonpolar solvents, we also prepared a few anions with longer alkyl substituents. In **38a** and **39a** (Chart

Scheme 4. Synthesis of Ethylated Anions^a

^a E': EtOTf and CaH₂ in sulfolane.

2), the carbon vertex carries an *n*-hexyl instead of a methyl group. Their synthesis is entirely analogous to those of **2a** and **16a**, respectively. Scheme 4 shows that the replacement of methyl triflate with ethyl triflate permitted a conversion of the 1-TIPS blocked anion **18a** into the hexaethylated derivative **40a** and hence into **41a**, an ethylated analogue of **11a**. Exhaustive ethylation of **11a** with ethyl triflate led to the undecasubstituted **42a**, analogous to **12a**. However, ethyl triflate in sulfolane failed to introduce 11 ethyl groups into **1a**, and we did not obtain the 1-H-undecaethyl anion previously reported¹⁵ from a high-temperature sealed-tube ethylation with ethyl bromide. In our hands, all alkylations attempted under these drastic sealed-tube conditions failed to give useful yields of pure products, primarily because of cage bromination.

Anodic Oxidation to Radicals. The electrochemical behavior of **1a–16a** has been examined by cyclic voltammetry in liquid SO₂, using techniques developed by Bard and collaborators.⁴⁵ This solvent dissolves the carborate salts well and has a large electrochemical window. Since we use a platinum quasi-

(45) Tinker, L.; Bard, A. *J. Am. Chem. Soc.* **1979**, *101*, 2316.

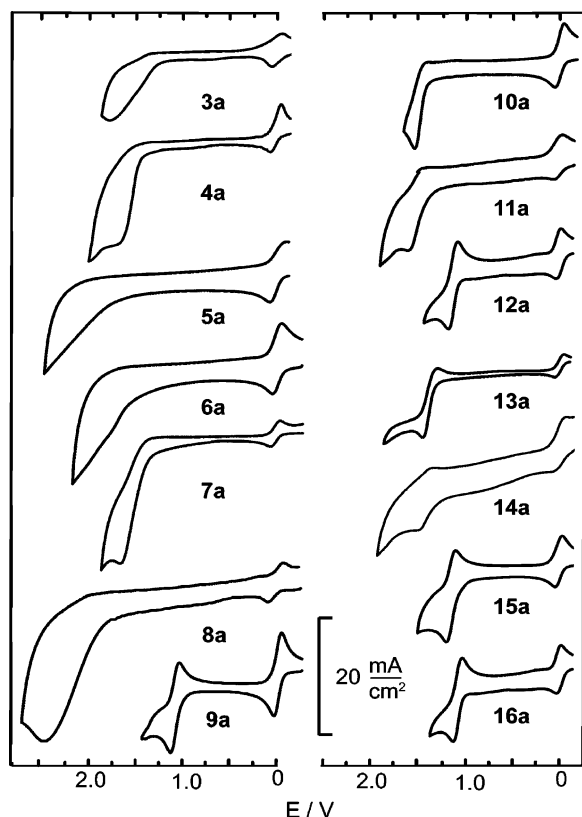


Figure 1. Cyclic voltammograms (first scans) in liquid SO₂ at 0 °C and 0.5 V/s, against ~3 mM Fc/Fc⁺ (~10–20 mM cesium carborate, ~0.1 M Bu₄NPF₆).

reference electrode instead of a real reference electrode, potentials are expressed relative to a ferrocene standard.

One-electron oxidation of the permethylated anion **16a** in acetonitrile is reversible and yields the stable and isolable neutral radical **16r**.²⁶ In contrast, guided by the results reported⁴⁶ for the related unsubstituted anions CB₉H₁₀⁻,²² B₁₀H₁₀²⁻,^{47–49} and B₁₂H₁₂²⁻,⁵⁰ we anticipate irreversible oxidation for those anions that carry no or only a few methyl groups and expect the resulting radicals to be unstable with respect to a multistep formation of a dimer of a hypercloso species with a deprotonated (“naked”) boron vertex.

We wondered how extensive the methylation needs to be before the neutral radical becomes stable and the electrochemical behavior of the anion becomes reversible. Reversibility is essential for many potential applications, and also for our present objective, an assessment of the effect of methylation on the redox potential. We anticipate performing a detailed electrochemical study of selected anions at a later time. For the moment, we have made no attempt to perform preparative electrolysis and to isolate and characterize the monomeric or dimeric final products of any of the oxidations.

The cyclic voltammograms are shown in Figure 1, and the half-wave reduction potentials $E_{1/2}$ of the reversible oxidations (and the peak potentials E_p of the irreversible ones) are summarized in Table 1. Clean chemically reversible behavior

is observed only for **9a**, **12a**, **13a**, **15a**, and **16a**. For these anions, the separation between the well developed anodic and cathodic peaks is comparable to that observed for ferrocene, which is at most 0.1 V. A vague but reproducible indication of a reduction peak can be discerned in the only slightly reversible cyclic voltammograms of **10a**, **11a**, and **14a**, for which the anodic/cathodic separation still is about 0.1 V. The values given for these anions are less accurate. The oxidation of **3a**, **4a**, **6a**, **7a**, and **8a** is strongly chemically irreversible. These anions do not show any reproducible reduction peak in the cyclic voltammogram at scan speeds up to 1 V/s. When the first cycle is recorded, the anodic/cathodic separation for ferrocene peaks is still no more than 0.15 V, but the electrode fouls rapidly. The values listed for **3a** and **6a**, which show only a hint of an anodic shoulder, are very approximate. Anions **4a** and **7a** show a more clearly defined anodic peak. Anion **8a** exhibits a very positive, strangely broad, and especially poorly reproducible peak, presumably due to rapid electrode fouling. We exclude it from any attempts at analysis, similarly as the anions **1a**, **2a**, and **5a**, which showed neither any oxidation wave up to the solvent limit, even when the supporting electrolyte was changed from Bu₄N⁺PF₆⁻ to Bu₄N⁺AsF₆⁻, nor any hint of a reduction peak. The anion **5a** seems to catalyze the oxidation of the supporting electrolyte or the solvent, since it shows a clear rise of anodic current at strongly positive potentials. A similar rise is observed with the anions **3a**, **6a**, and **8a**. None of the anions show any indication of further oxidation of the radical to a cation.

Thus, an increase in the number of methyl substituents generally favors not only a more facile but also a more reversible oxidation. Increased steric hindrance to bimolecular reactions undoubtedly helps, and it is not unusual to see a higher reversibility for the more easily oxidized members of a series. However, the positions of the substituents matter nearly as much as their number. What the reversibly oxidized anions have in common is the absence of a pair of adjacent unsubstituted BH vertices in positions 7–12. This structural feature is also present in the anions **4a**, **7a**, and **11a**, whose electrochemistry is not reversible, and this degree of steric hindrance may thus be necessary but is not sufficient for radical stability and electrochemical reversibility.

We shall see below that the redox potentials of the five reversibly oxidized anions (Table 1) correlate quantitatively with theoretical expectations when solvent effects are included explicitly. To determine whether the anodic oxidation of the irreversibly oxidized anions correlates at least roughly, we define their peak potentials as follows: for **10a**, **11a**, and **14a**, we use the average of the potential of the anodic peak and the ill-developed return peak (values in parentheses in Table 1), and for **3a**, **4a**, **6a**, and **7a**, we use the position of the anodic peak (values in brackets in Table 1).

Calculation of the Oxidation Potentials. Considering that methyl is normally viewed as a weakly perturbing substituent, the range of values observed for the anodic oxidation potentials of **1a**–**16a**, about 1 V, is notable. The carborane cluster cage clearly elicits considerable electron density donation by the methyl substituent. In spite of the large size of the molecules, quantum chemical calculations should be able to account for the reversible redox potentials quantitatively.

(46) Hawthorne, M. F.; Shelly, K.; Li, F. *Chem. Commun.* **2002**, 547.

(47) Hawthorne, M. F.; Pilling, R. L.; Stokely, P. F. *J. Am. Chem. Soc.* **1965**, *87*, 1893.

(48) Watson-Clark, R. A.; Knobler, C. B.; Hawthorne, M. F. *Inorg. Chem.* **1996**, *35*, 2963.

(49) Middaugh, R. L.; Farha, F., Jr. *J. Am. Chem. Soc.* **1996**, *88*, 4147.

(50) Wiersma, R. J.; Middaugh, R. L. *J. Am. Chem. Soc.* **1967**, *89*, 5078.

Table 1. Oxidation Potentials in SO₂(l) ($E_{1/2}$ or E_p in V against Fc/Fc⁺), Anodic/Cathodic Peak Separations (Δ , V), HOMO Energies (ϵ , eV), and Calculated Electron Detachment Energies (ΔE , eV)^a

anion	obsd		calcd					predicted	
	$E_{1/2}$ or E_p	Δ	- ϵ (HOMO)		ΔE (vert)			$E_{1/2}$	
			A HF/ 6-31+G*	B CASSCF(3,2)/ 6-31+G*	C B3LYP/ 6-31+G*	D RI-DFT(B-P)/ TZVP	E RI-DFT(B-P)/ TZVP-COSMO	F from E	G from increments
1a	—	—	6.40	5.24	5.45	5.24	6.93	2.00	1.82
2a	—	—	6.41	5.21	5.40	5.19	6.89	1.97	1.77
3a	[1.77]	—	6.02	4.80	5.02	4.85	6.37	1.58	1.48
4a	[1.63]	—	6.00	4.74	4.97	4.78	6.24	1.49	1.48
5a	—	—	6.41	5.21	5.24	5.04	6.69	1.82	1.81
6a	[1.74]	—	6.02	4.77	4.97	4.82	6.50	1.68	1.43
7a	[1.60]	—	6.01	4.72	4.93	4.76	6.30	1.53	1.43
8a	[2.46]	—	6.43	5.18	5.19	4.99	6.64	1.79	1.76
9a	1.09	0.09	5.73	4.42	4.65	4.47	5.77	1.14	1.14
10a	(1.49)	(0.11)	6.05	4.80	4.97	4.83	6.34	1.56	1.48
11a	(1.52)	(0.14)	6.02	4.73	4.97	4.69	6.12	1.40	1.47
12a	1.12	0.09	5.75	4.42	4.65	4.46	5.71	1.09	1.13
13a	1.37	0.15	6.02	4.70	4.83	4.64	6.07	1.36	1.42
14a	(1.41)	(0.12)	6.04	4.77	4.95	4.81	6.32	1.55	1.42
15a	1.14	0.10	5.73	4.40	4.63	4.44	5.75	1.12	1.09
16a	1.08	0.08	5.75	4.39	4.63	4.44	5.69	1.08	1.08

^a For details, see the Experimental Section. Method of calculation is given; the calculations are in vacuum, except for COSMO, where the solvent parameters were those for acetone. The geometries have been optimized. The predictions in columns F and G are based on least-squares regression lines. The empirical increments for replacement of a single methyl group with a hydrogen in positions 1, 2, 7, and 12 of **16a** are 0.052, 0.068, 0.070, and 0.009 V, respectively.

We first assume that the solvation energy differences among these large delocalized anions are small and that it is acceptable to ignore the differences in the geometries of the anions and the neutral radicals. This calls for the calculation of the vertical electron detachment energy (ΔE) of the anion in vacuum. The simplest approach is to use Koopmans' theorem and to equate ΔE with minus the energy of the highest occupied molecular orbital (HOMO). This is known to be subject to large absolute errors, but we are only interested in relative values for a set of closely related molecules. An advantage of this simple approach is that the interpretation of substituent effects on the redox potentials is intuitively understandable using perturbation theory and a pictorial representation of the HOMO.

Next, we consider explicitly the existence of geometrical differences between the anions and the radicals, accentuated by first- and second-order Jahn–Teller distortions in the latter, and evaluate δE from a difference of energies calculated in vacuum for the anion and the radical at the optimized geometry of each. Finally, we add an explicit consideration of solvation energies, and it will be only at this point that a satisfactory agreement with experiment will be reached.

Calculated Anion Geometries and Molecular Orbitals.

Molecular geometries of the anions **1a**–**16a** were optimized at the HF/6-31G*, HF/6-31+G*, and B3LYP/6-31+G* levels, with essentially identical outcomes. The geometries of all the anions are very similar, and the cages have a nearly exactly C_{5v} symmetry, perturbed only by the threefold symmetry of the methyl groups. Important geometrical parameters of anions **1a**, **8a**, and **16a** are listed in Table 2. We do not show the charge distribution or the electrostatic potential around the anion, since they were published recently.²⁸ In that study, we compared the natural atomic charges in **1a** and **16a** and concluded that a methyl group on boron had a σ -electron-withdrawing inductive effect relative to the hydrogen standard, in addition to its well recognized π -electron-donating effect. Electron withdrawal by a methyl on a neutral carborane cage has been recently emphasized by others.²⁴

Table 2. Calculated Geometrical Parameters of **1a**, **8a**, and **16a**^a

	HF/6-31+G*			B3LYP/6-31+G*		
	1a	8a	16a	1a	8a	16a
$d_{1,2}$	1.707	1.715–1.721	1.728–1.731	1.707	1.715–1.722	1.728–1.730
$d_{2,3}$	1.785	1.778–1.780	1.790–1.795	1.782	1.774–1.777	1.788–1.792
$d_{2,7}$	1.781	1.771–1.780	1.788–1.790	1.777	1.771–1.776	1.783–1.785
$d_{7,8}$	1.800	1.793–1.796	1.803–1.806	1.794	1.784–1.788	1.798–1.799
$d_{7,12}$	1.796	1.803–1.805	1.801–1.803	1.788	1.796–1.797	1.795–1.797
$\alpha_{2,1,3}$	63.0	62.3–62.4	62.3–62.5	62.9	62.1–62.3	62.2–62.5
$\alpha_{7,12,8}$	60.2	59.6–59.7	60.0–60.1	60.2	59.6–59.7	60.1
$d_{1,c}$	—	1.526	1.527	—	1.528	1.528
$d_{12,c}$	—	1.614	1.617	—	1.612	1.613
$d_{2,c}$	—	—	1.610–1.611	—	—	1.605–1.606
$d_{7,c}$	—	—	1.617–1.618	—	—	1.612–1.613

^a In Å; $d_{x,y}$ is the distance of vertices x and y ; $\alpha_{x,y,z}$ is the angle between lines xy and yz ; and $d_{x,c}$ is the distance from vertex x to the carbon of its methyl substituent.

Since there is arbitrariness in the definition of atomic and group charges, it is of interest to use other criteria for the evaluation of the substituent effect of the methyl group as well. The results of our computations provide such an opportunity. The trends in orbital energies of the various methylated derivatives at the anion equilibrium geometries are displayed in Figure 2. A qualitative rationalization of the regularities observed can be developed in terms of perturbation theory along the lines popularized by Dewar,⁵¹ permitting an independent evaluation of the substituent effect of the methyl group based on energy criteria alone. For this purpose, we first need to transform the MOs of the parent anion **1** to a locally symmetry adapted basis set. This will be useful in other contexts, too, e.g., for the understanding of interactions between carborate(–) anion icosahedra connected via conjugating groups.²⁹

Molecular Orbitals of 1a. The HF/6-31+G* MOs of the parent icosahedral B₁₂H₁₂^{2–} anion are similar to those derived from Stone's tensor harmonic bonding model.^{52–55} The HOMO

(51) Dewar, M. J. S.; Dougherty, R. C. *The PMO Theory of Organic Chemistry*; Plenum: New York, 1975.

(52) Wales, D. J.; Stone, A. J. *Inorg. Chem.* **1989**, *28*, 3120.

(53) Stone, A. J.; Wales, D. J. *Mol. Phys.* **1987**, *61*, 747.

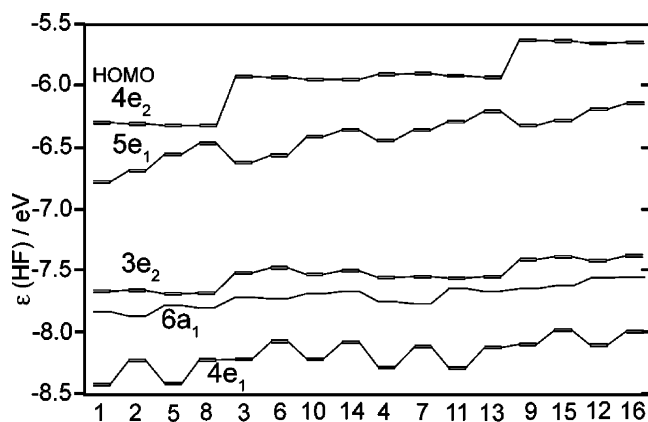


Figure 2. Calculated (HF/6-31G*) energies ϵ of the frontier orbitals of 1a–16a.

is a set of quadruply degenerate F^{π} orbitals of $1g_u$ symmetry, and the HOMO-1 is a set of quintuply degenerate D^{π} orbitals of $2h_g$ symmetry. The next 12 lower orbitals are principally the C–H and B–H bond orbitals, referred to as the *exo* orbitals. The last four valence orbitals are the strongly bonding $1 \times S^{\sigma}$ and $3 \times P$. The molecular orbitals of **1a** can be related to those of $B_{12}H_{12}^{2-}$ using the correlation between the I_h and C_{5v} point groups.⁵⁶ The occupied valence orbitals of $CB_{11}H_{12}^{-}$ can be divided into a frontier set (25 to 17), an *exo* bonding set (16 to 5), and a strongly bonding cluster set (4 to 1).

Stone⁵³ solved the SCF problem for $B_{12}H_{12}^{2-}$ in a Cartesian Slater-type basis symmetry adapted to the icosahedral geometry of the cluster. We adopt the same basis set, consisting of the valence atomic functions of the 12 nuclei hybridized to produce one inward and one outward pointing radial *sp* hybrid basis function and leaving two tangential *p* functions intact (Figure 3). The *z* axis is the fivefold symmetry axis, with the carbon atom (position 1) on the top. The *y* axis lies on a mirror plane. On the “equatorial” vertices 2–11, the axis of one tangential orbital lies in a plane containing the *z* axis and the other is parallel to the *xy* plane. One of the tangential orbitals located on the “axial” vertices 1(C) and 12(B) is directed along *x*, and the other, along *y*.

Unlike Stone, we perform a conventional DFT or *ab initio* calculation in a Cartesian GTO basis (6-31G* or 6-31+G*), calculate the density matrix, and transform the Cartesian basis into the cluster basis constructed from the valence portion of the orthonormal natural atomic orbital (NAO) basis⁵⁷ (the deleted Rydberg NAO functions had weights below 0.02 in each occupied MO). This general procedure will produce a set of MOs expressed in an orthogonal cluster basis from any initial calculation that yields a density matrix.⁵⁸

The nine frontier MOs of $CB_{11}H_{12}^{-}$ (Figure 4) are derived from the F^{π} and D^{π} MOs of $B_{12}H_{12}^{2-}$. For each of them, Table 3 gives the energy and symmetry (core orbitals are not counted in the numbering used), the total weight of the cluster basis orbitals, and the weight of each type of cluster basis orbital.

(54) Harmon, K. H.; Thomas, T. E.; Stachowski, B. M. *J. Mol. Struct.* **1995**, *350*, 135.

(55) Abe, J.; Shirai, Y. *J. Am. Chem. Soc.* **1996**, *118*, 4705.

(56) Nakamoto, K.; McKinney, M. A. *J. Chem. Ed.* **2000**, *77*, 775.

(57) Glendening, E. D.; Reed, A. E.; Carpenter, J. E.; Weinhold, F. *NBO*, version 3.1.

(58) The computer program needed for the transformation of NBO output to the cluster basis and for the preparation of the drawings is available in the Supporting Information.

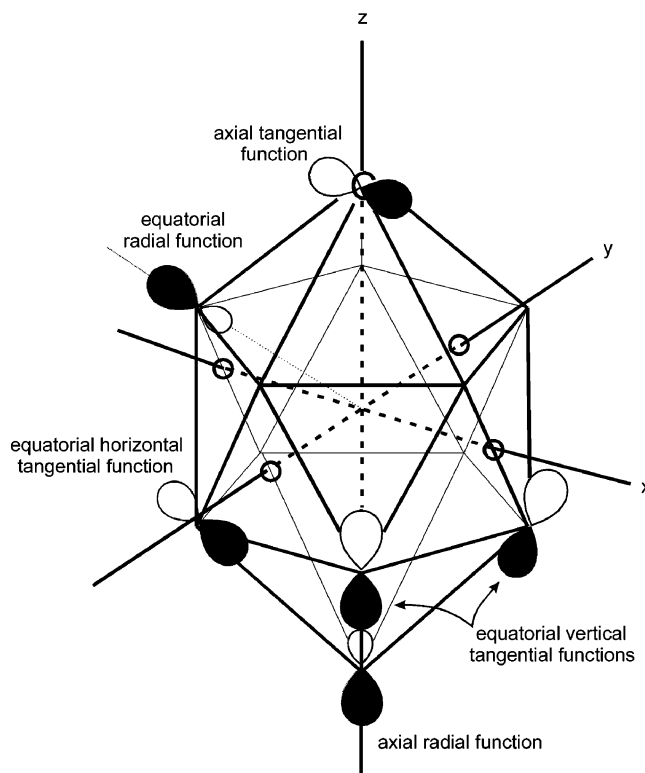


Figure 3. Definition of the cluster basis functions.

Since the cluster basis is orthogonal, the weights are equal to the sums of the squares of the linear combination of atomic orbital (LCAO) coefficients. The MOs are displayed in Figure 4 by showing the magnitudes and the signs of the contributions from the individual members of the cluster basis set in a perspective view of the icosahedron, taken from a point located near the positive segment of the *z*-axis, such that the vertex 1 (C, closer) projects a little below vertex 12 (B, farther). Lines connect the closest atomic contacts as usual. The radial lines emanating from the C(1) vertex connect to the five vertices of the proximate pentagon B(2–6), shown larger, and lines emanating from the B(12) vertex connect to the vertices of the distal pentagon, shown smaller.

The contributing basis set orbitals are not scaled with perspective. The horizontal tangential orbitals are drawn as lemniscates whose short diameter is proportional to their LCAO coefficients. The vertical tangential orbitals are drawn as offset circles whose diameter is proportional to their LCAO coefficients. Each is radially offset from its vertex to avoid obscuring other orbitals. The two equatorial radial functions are centered at the vertex, and in some cases, a lobe of an orbital is obscured by a lobe of the other. The largest short diameter of the unsymmetrical lemniscate is proportional to the LCAO coefficient. The radial functions at the axial positions are drawn as offset circles with different diameters, with the larger diameter proportional to their LCAO coefficient. These orbitals are horizontally offset from their vertex. The left orbital points from C(1) to B(12), and the right orbital, from B(12) to C(1). The two tangential functions at the axial position are drawn as lemniscates whose diameter is proportional to their LCAO coefficients.

The nine frontier MOs of $CB_{11}H_{12}^{-}$ all have contributions from H 1*s* functions, not shown in Figure 4. For a pure cluster MO, the weight *n* of the cluster basis functions would equal 1.

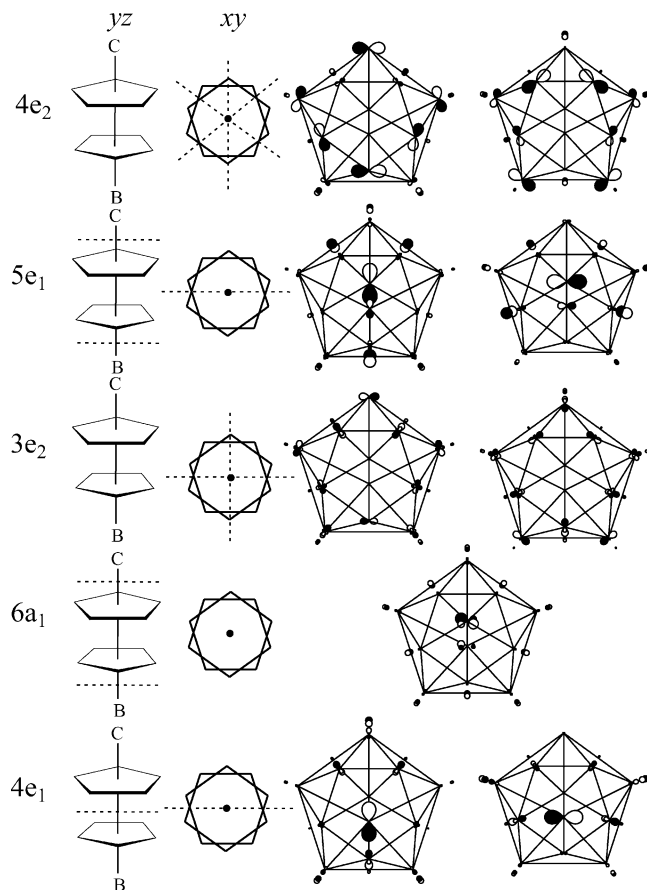


Figure 4. Occupied frontier MOs of **1a**. The left column gives the orbital label. The next two columns show the nearly horizontal and nearly vertical nodal surfaces of the MO immediately to the right. Dashed lines represent the intersection of the nodal surfaces with the yz plane and xy plane (see text). The next two columns are diagrams of the MOs, viewed from C(1) to B(12).

Table 3. Frontier Orbitals of **1a**^a

orbital	n^b	ϵ/eV	sym	AO class	population ^c			
					1	2–6	7–11	12
HOMO	0.99	-6.163	4e ₂	tang.	0	0.48	0.51	0
				rad.	0	0	0	0
HOMO-1	0.93	-6.632	5e ₁	tang.	0.1	0.12	0.42	0.24
				rad.	0	0.1	0.1	0
HOMO-2	0.7	-7.533	3e ₂	tang.	0	0.17	0.13	0
				rad.	0	0.17	0.23	0
HOMO-3	0.7	-7.689	6a ₁	tang.	0	0.11	0.17	0
				rad.	0.1	0.1	0	0.27
HOMO-4	0.72	-8.278	4e ₁	tang.	0.22	0.12	0	0
				rad.	0	0.1	0.26	0

^a HF/6-31+G*. Core orbitals are not included in MO numbering. ^bTotal cluster basis population (the remainder is in H orbitals). ^cNormalized to unity for each member of each degenerate pair.

Table 3 shows that the doubly degenerate HOMO (4e₂) and HOMO-1 (5e₁) frontier MOs are nearly pure cluster orbitals and have very little contribution from the H 1s functions, while the lower lying 3e₂, 6a₁, and 4e₁ frontier MOs have a larger contribution from H 1s functions and participate in BH bonding.

The members of the degenerate HOMO (4e₂) orbital pair are almost entirely composed of horizontal tangential basis functions at the equatorial positions, with nearly equal weights of the tangential functions on the two pentagons (Table 3). In each member of the pair, large coefficients are concentrated on one side of the proximate pentagon and the opposite side of the

distal pentagon. The HOMO contains three vertical nodal surfaces (Figure 4) and is of φ symmetry with respect to the fivefold axis. Symmetry precludes any contributions from s , p , or d valence orbitals at the axial vertices. Only the equatorial positions of substitution provide valence interaction opportunities with the HOMO for atoms of elements of main or transition metal groups of the periodic table.

The members of the degenerate HOMO-1 (5e₁) orbital pair have their amplitude concentrated in the lower hemisphere (Figure 4). They contain a large purely tangential contribution at B(12) and a small parallel contribution at C(1), as well as significant vertical tangential contributions at the distal pentagon. These MOs have one vertical nodal surface and π symmetry with respect to the rotation axis. They are particularly well suited for interaction with π -type p orbitals of substituents in position B(12). As would be expected from their F ^{π} provenance, they also have two horizontal nodal surfaces, one between C(1) and B(2–6) and one between B(12) and B(7–11). The antipodal effect in the NMR spectra of 12-vertex boranes and carboranes has been attributed to these orbitals.⁵⁹

Like the 4e₂ MOs, the δ symmetry 3e₂ orbitals are confined to the equatorial vertices B(2–11) (Figure 4) and contain horizontal and vertical tangential functions as well as radial ones. They, and the next MOs, are of D ^{π} provenance and contain two nodal surfaces. In 3e₂, they are both vertical. The σ symmetry 6a₁ orbital has the largest contributions from the radial functions at the axial positions, particularly B(12). Its two nodal surfaces are horizontal, between positions C(1) and B(2–7) and between positions B(12) and B(7–11). By symmetry, horizontal tangential functions do not contribute, but the vertical ones do, particularly at the distal pentagon. The π symmetry 4e₁ orbitals are a counterpart to the 5e₁ MOs but are concentrated in the upper hemisphere. The contribution at C(1) is tangential and antiparallel to the very small contribution at B(12). These orbitals have one vertical nodal surface and a horizontal nodal surface that lies between the two equatorial pentagons.

We note that eight out of the nine topmost occupied MOs of the three-dimensionally conjugated **1a** have only tangential amplitude (or none) at each vertex, and local symmetry constrains them to interaction with π -symmetry orbitals of substituents. Among the occupied MOs of **1a**, only those of very low energy can interact with σ -symmetry orbitals of substituents. In this regard, the former are like the occupied π MOs and the latter like the occupied σ MOs of the common two-dimensionally conjugated planar systems, in which the constraint is forced by global symmetry.

Anodic Oxidation Potentials and MO Energies. Table 1 gives the HF/6-31+G* HOMO energies calculated for **1a–16a**. The HF/6-31G* and HF/6-31+G* results for HOMO energies are closely correlated, $\epsilon_{\text{HOMO}}(6-31+G^*) = 0.970\epsilon_{\text{HOMO}}(6-31G^*) - 0.327$ (eV, $R^2 = 1.000$). The HOMO energies cluster around only three distinct values (Figure 2), -5.74 ± 0.02 (group I), -6.02 ± 0.03 (group II), and -6.41 ± 0.01 eV (group III). Group I comprises those with 10 methyl groups in the equatorial positions 2–11, group II, those with only 5, and group III, those with none. Methyl groups in the axial positions 1 and 12 play no role at all.

A comparison with the experimental redox potentials produces mixed results (Figure 5A). All four anions in group I, **9a**, **12a**,

(59) Connely, N. G.; Geiger, W. E. *Chem. Rev.* **1996**, *96*, 877.

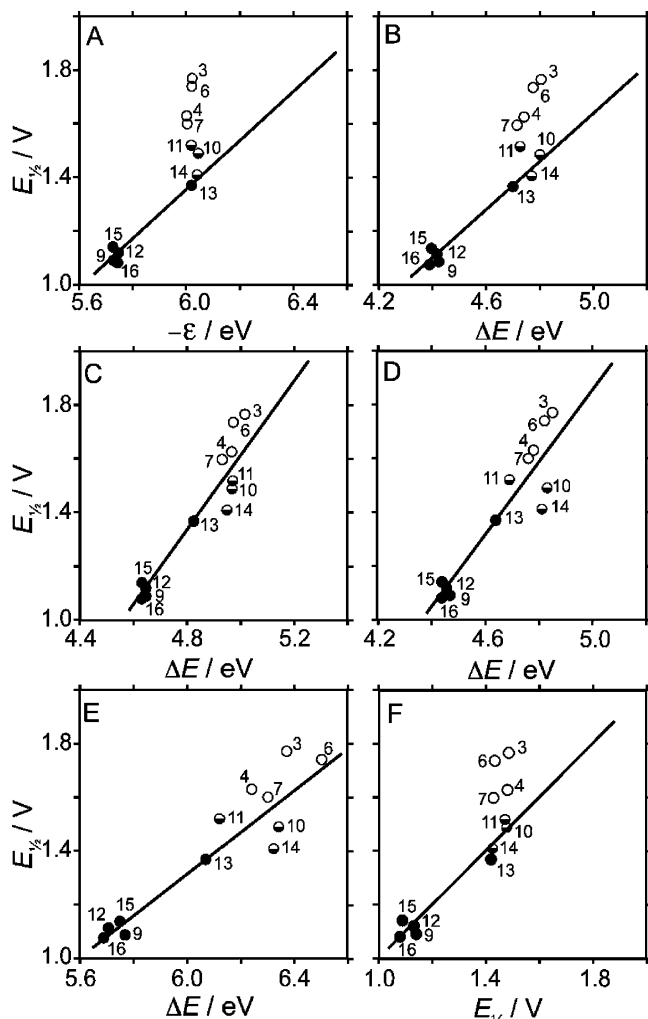


Figure 5. Measured (y) vs computed (x) oxidation potentials. Full circles, reversible; half-full circles, partly reversible; empty circles, fully irreversible oxidation. In A–E, the regression line was fitted to reversible data only. In F, it was fitted to the reversible and semireversible data and forced to pass through point for **16a**. A: $-\text{HOMO}$ energy of anion (HF/6-31+G*), $y = 0.92x - 4.18$, $R^2 = 0.95$; B: vertical electron detachment energy (CASSCF/6-31G*), $y = 0.89x - 2.82$, $R^2 = 0.95$; C: adiabatic electron detachment energy (B3LYP/6-31G*), $y = 1.39x - 5.34$, $R^2 = 0.95$; D: adiabatic electron detachment energy (RI-DFT(B-P)/TZVP), $y = 1.36x - 4.94$, $R^2 = 0.92$; E: adiabatic electron detachment energy (RI-DFT(B-P)/TZVP, COSMO, solvation in acetone), $y = 0.75x - 3.18$, $R^2 = 0.94$; F: increment model fitted to reversible and partly reversible data, $y = 0.98x + 1.08$, $R^2 = 0.98$.

15a, and **16a**, provide reversible peaks and reliable redox potentials, but their spread over 0.06 V is not at all reproduced by the calculated HOMO energies. On the other hand, the 0.26 V difference of their average redox potential and the redox potential of **13a**, the only reversible anion of group II, is nearly equal to the calculated difference of average HOMO energies of groups I and II. Another shortcoming of this theoretical approach is that, among the three anions of group II that exhibit at least some indication of reversibility, **14a** is about as easy to oxidize as **13a**, as expected from the HOMO energies, but **10a** and **11a** are 0.2 V harder to oxidize, and this is not suggested by the calculated HOMO values at all. This discrepancy may possibly be due to the distortion of peak positions by irreversibility. The other anions of the second group II all give entirely irreversible waves, and the potentials of their oxidation peaks vary widely but tend to be high, as expected from the HOMO

energies. Only one anion of group III (**8a**) yields an oxidation wave, and its potential is very high as expected, but fully irreversible. It thus appears likely that the calculated HOMO energies reflect the average difference between at least two of the three groups of anions fairly correctly but do not reproduce the more subtle differences within each group.

Perturbation MO Treatment of Substituent Effects. We are particularly interested in rationalizing the effect of substituents on the degenerate HOMO and the degenerate HOMO–1, relevant for anodic oxidation and for applications of frontier orbital theory to electrophilic substitution. Both the HOMO and the HOMO–1 must be considered for these purposes, since they are both related to the F^π HOMO set of the parent icosahedral B₁₂H₁₂²⁻ dianion and are close in energy.

We shall use a slight generalization of Dewar's perturbation MO treatment of substituent effects,⁵¹ based on the Hückel Hamiltonian, which was developed for planar π -electron systems. It treated field effects by first-order perturbation theory, which describes the change ΔE_i in the energy of the i -th MO by the expression

$$\Delta E_i = \sum_m C_{mi}^2 \Delta \alpha_m \quad (1)$$

where C_{mi} is the expansion coefficient of the i -th MO on basis orbital m whose Coulomb integral (electronegativity) has changed by $\Delta \alpha_m$ as a result of substitution. This equation accounts for the energy order of $4e_2$ and $5e_1$ MOs of CB₁₁H₁₂⁻, both of which originate in the g_u HOMO of B₁₂H₁₂²⁻. The conversion of a B atom into a C atom in position 1 by addition of a proton into the nucleus makes $\Delta \alpha_1$ negative. Since the coefficients of the $4e_2$ orbital in position 1 vanish, while the $5e_2$ MO has considerable weight at this vertex (0.05, Table 3), the latter is stabilized preferentially. The other 11 vertices are more distant from the added positive charge and play a subordinate role. The order of the $3e_2$, $6a_1$, and $4e_1$ orbitals can be rationalized similarly.

To understand substitution effects resulting from the replacement of a hydrogen atom in CB₁₁H₁₂⁻ with methyl, we need to consider both the inductive (σ -symmetry) and the hyperconjugative (π -symmetry) effects of the methyl group. A recently published²⁴ discussion of a net electron-withdrawing effect appears to involve a misunderstanding. It emphasizes the large difference between the electronegativities of carbon and boron, but this is irrelevant for the usual definition of a substituent effect as the effect of the replacement of H with another group, in this case CH₃. It is only the difference between the electron density withdrawal from boron by H and by CH₃ that matters, and this difference is smaller. From a comparison of natural atomic charge distributions in **1a** and **16a**, we concluded²⁸ that, relative to hydrogen, the methyl group has an electron-withdrawing σ (inductive) effect, which probably does not propagate very far. The existence of the donor π (conjugative) effect of a methyl group on the skeleton of **1a**, which propagates farther, has been well recognized for a long time. It is reflected for instance in the much lower oxidation potential of **16a** as compared with **1a**.¹³ However, the π -donor effect of the methyl substituent on MO energies of **1a** (Figure 2) is only latent in that the interaction is of the occupied–occupied type and does not contribute to a net charge transfer to the cage to first order. The π -donor effect of the methyl substituent is revealed in **1r**,

where this group indeed delivers considerable electron density from its occupied π orbital to the singly occupied MO of the cage.

In addition to a qualitative consideration of atomic charges, we can now evaluate the σ and π effects of the replacement of a hydrogen atom by a methyl group quantitatively from its effect on the energies of the occupied valence MOs. It is immediately apparent that the effects of π hyperconjugation dominate. The HOMO and HOMO–1 set of orbitals interact with substituents only by π interactions, by symmetry. Only the $6a_1$ orbital, which possesses a significant radial contribution at position 1, is stabilized by a CH_3 group at that position, e.g., **1** vs **2** and **5** vs **8** in Figure 2. Even here, the effect is very small. The energy of all five valence orbital pairs increases with an increasing number of methyl groups. If σ symmetry inductive electron withdrawal were important, the introduction of methyl groups would stabilize an orbital. Field effects also appear negligible. Note, for instance, that the calculated energy of the $3e_2$ MO, which has no tangential contributions in positions 1 and 12, is not significantly affected by methyl substitution in these positions.

A quantitative treatment confirms these preliminary considerations and provides a rationalization of the trends observed in Figure 2. Delocalization effects due to a substituent S with orbitals of energy E_k^S and coefficients C_{pk}^S at the AO p (through which it interacts with the substrate R) on the energy E_i^R of an MO of a substrate R with coefficients C_{qi}^R at the AO q (through which it interacts with substituent) are described by the second-order perturbation expression⁵¹

$$\Delta E_i^R = \sum_k \frac{(C_{qi}^R)^2 (C_{pk}^S)^2 \beta_{pq}^2}{E_i^R - E_k^S} \quad (2)$$

Here we have assumed that each substrate MO/substituent MO interaction occurs through substrate AO (q)/substituent AO (p) resonance integrals at a single site. An obvious generalization would be needed if cyclic interactions were present.

In considering the introduction of a methyl substituent at one of the axial vertices of **1a**, or five such substituents at one of the two sets of equivalent equatorial vertices, we consider only the degenerate HOMO of the methyl group, whose two members are each represented by a π -symmetry combination of CH bonding orbitals that is symmetry adapted for interaction with one of the two tangential orbitals of the substituted vertex, and obtain

$$\Delta E_i^R = \frac{1}{E_i^R - E_k^S} (C_{pk}^S)^2 \beta_{pq}^2 \sum_q (C_{qi}^R)^2 \quad (3)$$

The only variables on the right-hand side of eq 3 are the orbital energy differences $E_i^R - E_k^S$ and the sum of the squares of the coefficients of the tangential cluster functions over the perturbed sites q , since the resonance integral β_{pq} and the methyl LCAO C_{pk}^S coefficient are constant. The validity of the second-order perturbation approximation is tested in Figure 6, in which the difference in the calculated energies of a given MO of $\text{CB}_{11}\text{H}_{12}^-$ and the corresponding orbital of a methylated cluster, ΔE_i^R , are plotted against sums of the squares of the coefficients of the tangential cluster AOs at the substituted sites, $\sum_q (C_{qi}^R)^2$.

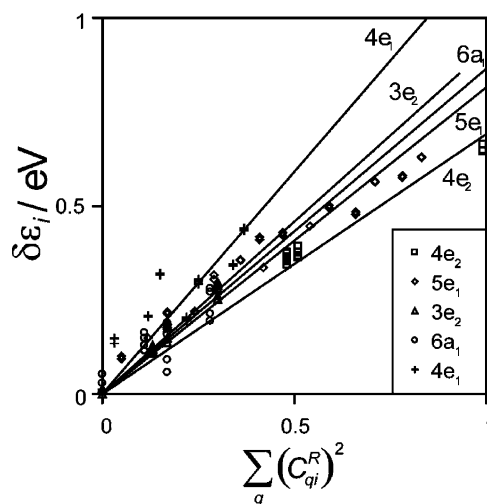


Figure 6. Correlation between the change in orbital energy due to methylation $\Delta \epsilon_i$ and the sum of the squares of the tangential orbital coefficients at the sites of perturbation, $\sum_q (C_{qi}^R)^2$.

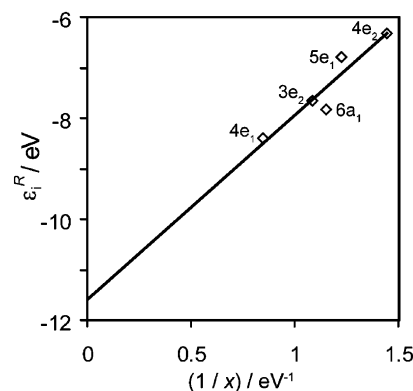


Figure 7. Correlation of unperturbed orbital energies and the reciprocal of the slope x of the lines from Figure 6. Slope: $C_{pq}^S \beta_{pq}^2$. Intercept: E_k^S .

The energy of the orbitals correlates ($R^2 = 0.98$ for all data) with the sum of the squares of the tangential orbitals at the methylated positions.

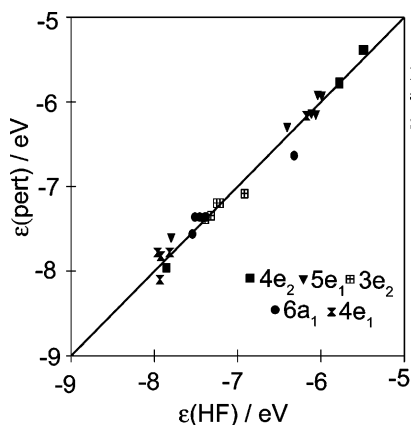
The slopes of the lines in Figure 6, equal to $(E_i^R - E_k^S)^{-1} (C_{pk}^S)^2 (\beta_{pq})^2$, vary as expected. Cluster MOs with energies close to the energy of the interacting orbitals of the methyl substituent are most strongly influenced. A plot of the reciprocal of the slopes from Figure 6 against the energies of the corresponding orbitals of **1a** is shown in Figure 7. The relationship is linear ($R^2 = 0.89$), and the slope, $(C_{pk}^S)^2 (\beta_{pq})^2$, has a value of 3.6 eV^2 . The energy of the occupied orbital of the methyl fragment, E_k^S , is given by the intercept and has a reasonable value of -11.6 eV .

In this approximation, eq 3 can be used for estimating the relative energy of a frontier orbital ΔE_i^R for any methylated derivative of **1a**, symmetric or not, by using the appropriate values of the unperturbed orbital energy E_i^R and sum of the squares of the tangential cluster C_{qi}^R coefficients (Table 4), and the above values of $(C_{pk}^S)^2 (\beta_{pq})^2$, and E_k^S . The orbital energies for anions **1a–16a** predicted by this second-order perturbation approximation correlate well with the actual SCF orbital energies (Figure 8; the slope of the regression line is 1.00 and R^2 is 0.98).

We made a similar attempt to simultaneously fit both the π symmetry hyperconjugative and the σ symmetry inductive effects of the methyl group. The latter depends on the amplitudes

Table 4. Predicted Effects of H → Me Substitution on the Energies of the Occupied Frontier Orbitals of **1a** (eV)^a

orbital	position			
	1	2–6	7–11	12
4e ₂	0	0.38/5	0.40/5	0
5e ₁	0.01	0.11/5	0.37/5	0.21
3e ₂	0	0.19/5	0.15/5	0
6a ₁	0	0.13/5	0.20/5	0
4e ₁	0.32	0.14/5	0.04/5	0

^a Values per substituent; division by 5 is indicated where needed.**Figure 8.** Orbital energies (eV): from perturbation theory and from HF calculation.

of the radial components of the cluster basis set and was handled in a manner similarly as the π term. The treatment yielded a very small destabilizing (electron donating) inductive term in addition to an almost unchanged π term and did not produce a statistically significant improvement over the results obtained with the latter alone. Using the topmost occupied orbital energy criterion for the evaluation, we conclude that the σ (inductive and field) effects of the methyl group relative to the hydrogen standard are negligible compared with the π effect. This is entirely in accordance with the above characterization of the topmost occupied MOs as locally π in nature. The relation of this result to our previous conclusion that methyl acts as a σ -electron acceptor,²⁸ based on a qualitative consideration of natural charges is not simple. We have already noted above that the occupied–occupied orbital interactions that are of primary interest presently do not cause net charge transfer between the substituent and the cage to first order. It seems clear that the effect of replacement of a hydrogen by a methyl on observable properties of cage boranes that are dictated primarily by the topmost occupied MOs will be interpretable with π effect alone, without reference to the σ effect. On the CB₁₁ cage, the methyl group acts as a π donor, and hyperconjugation with its CH bonds outweighs hyperconjugation with its CH antibonds. However, this does not mean that on a substrate with a higher energy HOMO, perhaps already on B₁₂H₁₂²⁻, it could not be a π acceptor, especially in the gas phase.

For substituents of lower symmetry, such as OH or NH₂, located in an equatorial position 2–11, the interaction with the two tangential AOs of the substituted vertex would in general not be the same, and rotation about the substituent–vertex bond would modulate the interaction similarly as it does in a substituted benzene. The effect on the HOMO (HOMO–1) will

be the largest if the axis of the substituent p donor orbital is horizontal (vertical).

Equation 1 suggests that it might be possible to define additive increments for the effect of a methyl group in positions 1, 2, 7, and 12 on the redox potential in a purely empirical fashion. If this is done by least-squares fitting to the reversible and partly reversible potentials (the reversible potentials by themselves are insufficient to obtain all four increments), using **16a** as the reference point, the increments are 52, 68, 70, and 9 mV, respectively. These values are in excellent agreement with theoretical expectations (Table 4) except for position 1, where the methyl group has more effect than it should. This might be related to the Jahn–Teller distortion discussed below. The results and predictions for all other anions based on the regression line (Figure 5F) are listed in Table 1.

Calculation of Vertical Electron Detachment Energies. An alternative to using Koopmans' approximation is to calculate the energies of the anion and the radical separately at the optimized geometries of the anions and to take their energy difference to obtain the vertical electron detachment energy. The 6-31+G* Hartree–Fock results discussed above have been used for the anions. However, since their HOMOs are degenerate at the 5-fold symmetric vertical geometry (or nearly degenerate if a methyl group is present in positions 1 and/or 12), the simplest valid approximation that can be used for the radical ground state employs a two-configuration wave function, CAS(3,2), using the same basis (Table 1). For parent **1r**, we have repeated the calculations at the CAS(13,12) level and found that the CAS(3,2) approximation is justified.

The results are very similar to those obtained in the Koopmans approximation in that they render correctly the large difference between the average redox potentials in group I and that of **13a**, the only reversibly oxidized anion of group II, but again fail to reproduce the small differences within group I (Figure 5B). The problem thus is not due to the assumptions inherent to the use of the Koopmans theorem. Its next likely source is the degeneracy of the HOMO of the anions, which causes the neutral radicals to be Jahn–Teller distorted. If the various radicals distort and stabilize to different degrees, the observed adiabatic redox potentials need not correlate with the calculated vertical ones.

Jahn–Teller Distortion of the Radicals. One might hope that the methyl substituents represent a small enough perturbation that the first-order Jahn Teller effect will be similar in all of the radicals. The observation of very low-lying excited states in the radical **16r**²⁶ suggests that a second-order Jahn–Teller effect may be important as well. Since the HOMO–1 energies (Table 1, Figure 2) indicate that the (HOMO, HOMO–1) energy gap varies greatly across the series of anions, the magnitude of the second-order stabilization is unlikely to remain the same. We have therefore concluded that an explicit calculation of adiabatic electron detachment energies is needed and requires a geometry optimization for each of the 16 radicals. In order to determine whether this can be done reliably using a single-configuration based method, we first examined the Jahn–Teller effect in **1r** and some of its methylated derivatives at the state-average CASSCF(13,12)/6-31+G* level. We found that, at the geometries of the minima, a single configuration indeed describes the ground state adequately. The results for **1r** are described in detail next (Figure 9).

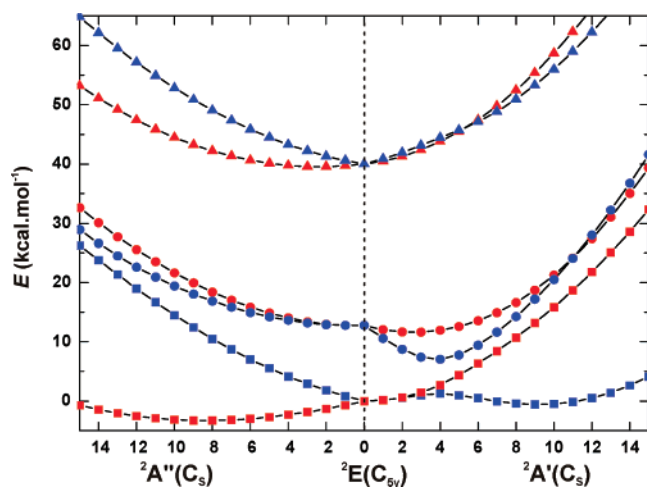


Figure 9. State-average CASSCF(13,12)/6-31+G* potential energy curves of the Jahn–Teller distortions of **1r**. Symmetry restricted geometry optimization was done at point 0 (C_{5v}) and both points 10 (C_s) for ${}^2A'$ (blue) and ${}^2A''$ (red) electronic states. Molecular geometries at the other points were interpolated (extrapolated) in the Cartesian coordinates of aligned C_{5v} and C_s minima.

Optimization of the ground state geometry of **1r** under constraint to C_{5v} symmetry (point 0) yields a doubly degenerate ground state wave function of E_2 symmetry, described well (coefficient is 0.96) by a pair of configurations derived from the HF wave function of **1a** by removal of an electron from one or the other orbital of the HOMO ($4e_2$) pair. At this geometry, the first excited state is only 13 kcal/mol higher. It is of E_1 symmetry and results from a removal of an electron from the HOMO–1 ($5e_1$) orbital of **1a** (coefficient 0.97). The next vertical state is 40 kcal/mol higher, is of E_2 symmetry, and results from a removal of an electron from the HOMO–2 ($3e_2$) orbital of **1** (coefficient 0.96).

Under C_s constraint, two distinct distortions of the ground state of **1r** lead from the fivefold symmetrical geometry to two distinct minima. In both minima, the CAS calculation shows a single dominant reference configuration, and an analysis of the Hessian matrix obtained from an HF calculation showed that these are true minima. The distortions split the triply occupied $4e_2$ orbital pair into a' and a'' orbitals and the 2E_2 ground state into ${}^2A'$ and ${}^2A''$ states. If the retained symmetry plane is chosen to be vertical on the right-hand side of Figure 4, in one of these distortions the two pentagons in the molecule are compressed horizontally and in the other, vertically, while expanding in the other direction. The horizontal compression (and vertical expansion, left of point 0 in Figure 9) places the symmetric a' orbital below the antisymmetric a'' orbital in energy and leads to an electronic $(a')^2(a'')$ ground state of ${}^2A''$ symmetry. The minimum in this state (point 10 on the left in Figure 9) is reached on a downhill path from the C_{5v} geometry (point 0). At the geometry of this minimum, the a' and a'' orbitals are very similar to the $4e_2$ HOMO pair of **1a** (Figure 4). The horizontal compression destabilizes the other component of the original 2E_2 ground state, the $(a')(a'')$ ${}^2A'$ state, and both components of the original 2E_1 excited state.

The vertical compression (and horizontal expansion, right of point 0 in Figure 9) leads to the other minimum, in which the electronic ground state is of ${}^2A'$ symmetry. This distortion splits and destabilizes both the ${}^2A'$ and the ${}^2A''$ component of the original 2E_2 ground state and thus would appear to have no

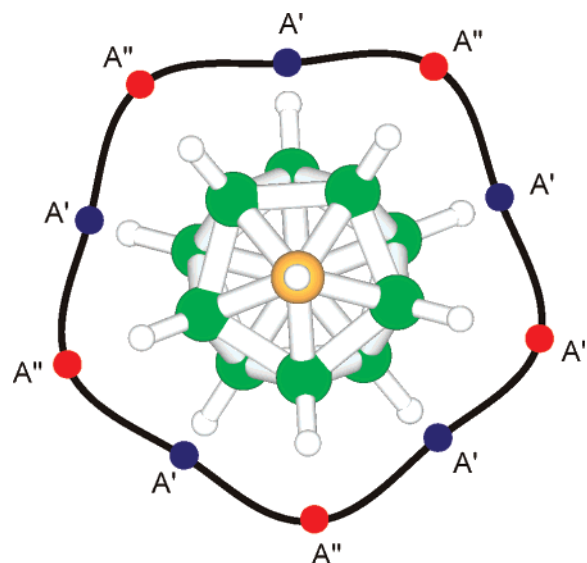


Figure 10. Schematic representation of the five pairs of ${}^2A'$ and ${}^2A''$ minima in the potential energy surface of **1r** surrounding the conical intersection at optimized C_{5v} geometry, and of the low-energy path connecting them.

opportunity to lead to a minimum in the ground state potential. However, it stabilizes both components of the original first excited 2E_1 state. One of them (${}^2A'$) is stabilized so strongly that it undergoes an avoided crossing with the ${}^2A'$ component originating from the original 2E_2 ground state and produces a ground-state minimum that is separated from the original C_{5v} point by a barrier. At the geometry of this minimum, the wave function of the ${}^2A'$ ground state is reminiscent of that of the ${}^2E'$ excited state of the C_{5v} symmetric geometry, in that the singly occupied MO looks like the a' component of the $5e_1$ orbital in Figure 4 and has a large amplitude on the antipodal B(12) atom.

Since the C_{5v} optimized structure contains five symmetry-equivalent mirror planes, there actually are five ${}^2A'$ and five ${}^2A''$ minima in the valley surrounding the conical intersection located at C_{5v} symmetry, one every 36° , as indicated schematically in Figure 10. At the present level of calculation, the ${}^2A''$ minima lie 2.7 kcal/mol below the ${}^2A'$ minima, but a few tests rapidly showed that this small difference is not calculated reliably and depends on the level of calculation. We have therefore made no attempt to calculate the undoubtedly small size of the 10 barriers that separate the 10 minima in the “Mexican hat” shaped potential energy surface and only indicated the low-energy path around the conical intersection schematically in Figure 10. The situation is even more complex than indicated so far, since it is likely that there are five additional conical intersections in the close vicinity of the five avoided crossings found at C_s geometries (Figure 9). Thus, **1r** may well be one of the more complicated cases of a Jahn–Teller induced conical intersection, with 10 local minima and 5 subsidiary conical intersections.

Calculation of Adiabatic Electron Detachment Energies in Vacuum. Since the CAS calculations on **1r** showed that the Jahn–Teller distorted radical is described well by a single-configuration wave function, we used single-configuration density functional theory (DFT) to obtain the ground state energies of the radical and the anion at their respective optimized geometries. Introduction of methyl substituents perturbs the symmetry of the states only a little, and the minima can still be

characterized as having an approximately ²A' or ²A'' ground state. In all radicals **1r**–**16r**, B3LYP/6-31+G*, RI-DFT(B-P)/TZVP, and HF/6-31+G* geometry optimizations yielded structures shown to be true minima by analysis of the corresponding Hessian at the HF/6-31+G* level, and the approximate ground state symmetry was ²A''. There seems to be little doubt that travel among the minima will be facile even at low temperatures, and the Jahn–Teller effect might be dynamic. This may well be the underlying cause of our failure to saturate the EPR signal of **16r** in a failed attempt to measure an ENDOR spectrum.²⁶

The resulting adiabatic electron detachment energies (Table 1) obtained with the B3LYP/6-31+G* (column C) and the RI-DFT(B-P)/TZVP (column D) methods do not correlate with the reversible redox potentials within anions of group I substantially better than the vertical energies of columns A and B do (Figure 5C,D). The adiabatic energies considerably overestimate the difference between the average redox potential of the anions of group I and that of **13a**, the only reversibly oxidized anion of group II, whereas the vertical energies underestimate it somewhat.

Calculation of Adiabatic Electron Detachment Energies in Solution. The somewhat unsatisfactory results shown in parts C and D of Figure 5 leave a final opportunity for improving the theoretical treatment, which is the inclusion of solvent effects. This was done using the RI-DFT(B-P)/TZVP method of calculation and the COSMO continuum model. Since the COSMO parameters for liquid SO₂ ($\epsilon = 17.6$) are not available, we used the values for acetone ($\epsilon = 20.7$).

At this level of treatment, finally, the small differences among the anions of group I are reproduced better, although **9a** still deviates somewhat. The slope of the regression line in Figure 5E is now much less than unity (0.75), whereas it was too high in Figure 5C and D. The correction for the solvent effects thus seems to be exaggerated. This is probably due to a combination of the approximations inherent to the COSMO model and to the use of acetone instead of liquid sulfur dioxide as a solvent in the calculation. Nevertheless, it appears that the inclusion of solvent effects is important for the calculation of relative redox potentials from adiabatic electron detachment energies.

The values predicted by the regression line for those anions that are oxidized irreversibly are listed in column F of Table 1. The peak positions observed for these anions fall within 0.2 V of the regression line in Figure 5E, suggesting that even these irreversible anodic peaks provide a rough indication of the value of the reversible redox potential.

Conclusions

All 15 symmetrically methylated derivatives **2a**–**16a** have now been prepared from **1a**, and the tools developed for their synthesis promise to be useful for the selective preparation of other derivatives of this parent anion. The one-electron oxidation potentials of the anions have been measured in liquid sulfur dioxide. Three of the anions cannot be oxidized under these conditions. Many of the others, especially all those with at least two adjacent BH vertices in positions 7–12, are oxidized irreversibly. The redox potentials of the five anions that are oxidized reversibly have been interpreted at several levels of theory. A simple empirical additive increment set accounts for the results qualitatively. When Jahn–Teller distortion of the radicals and the solvent effects are included in a DFT calculation

explicitly, the correlation with experiment is quite satisfactory and permits a prediction of the reversible potentials of the irreversibly oxidized anions. The conical intersection associated with the Jahn–Teller distortion of **1r** is very complicated, with five pairs of symmetry-related minima and, most likely, five additional conical intersections.

A description of the anions **1a**–**16a** in terms of the symmetry-adapted cluster basis set provides intuitive insight and permits a simple rationalization of the effects of methyl substitution on MO energies. We find that the methyl group has a significant π electron (hyperconjugative) donor effect and a negligible σ electron (inductive, field) effect on these energies, relative to the hydrogen standard.

Experimental Section

General. Unless stated otherwise, all synthetic procedures used standard inert-atmosphere techniques. THF and Et₂O were distilled from Na/benzophenone, sulfolane (tetramethylene sulfone) was vacuum distilled from CaH₂. Methyl and ethyl triflates were prepared according to a published procedure.⁶⁰ Other chemicals were reagent grade and used as purchased (triflic acid, 3M; other reagents, Aldrich). Me₃NH⁺I⁻ was prepared as described⁶¹ or purchased from Katchem Ltd. (E. Krásnohorské 6, 11000 Prague 1, Czech Republic). The ¹¹B NMR spectra were measured at 96.2 MHz. ¹H and {¹¹B} ¹³C NMR spectra were measured at 500 and 160.4 MHz, respectively. Peak assignments are based on ¹¹B COSY, ¹H–¹¹B HETCOR, and continuous wave {¹¹B} ¹³C NMR experiments. ¹H chemical shifts were measured relative to the residual protons from acetone-*d*₆ and referenced to Me₄Si. ¹³C chemical shifts were measured relative to ¹³C in acetone-*d*₆. ¹¹B chemical shifts were measured relative to BF₃·OEt₂, with positive chemical shifts downfield, using a B(OCH₃)₃ external standard (18.1 ppm). UV spectra were measured with a diode array spectrometer in spectral grade quality solvents. Mass spectra were recorded with an ESI, a VG 7070 EQ-HF Hybrid Tandem, and a GC–MS Ion Trap mass spectrometer. An HPLC system using C₁₈ columns (250 mm × 4.6 mm, 5 μ) with MeOH/water (1% AcOH, 0.7% Et₃N modifier) as the mobile phase was used for monitoring reactions. Larger columns (25 mm × 100 mm) were used for preparative separations.

Calculations. Hartree–Fock and B3LYP calculations were performed using Gaussian 03, revision B.02.⁶² Complete active space self-consistent field (CASSCF) calculations were performed using Molcas version 6.4.⁶³ All other calculations have been carried out with Turbomole 5.7 software.⁶⁴ Full DFT⁶⁵ geometry optimizations were performed with the Becke–Perdew (BP) density functional^{66,67} with the TZVP⁶⁸ quality basis set using the RI approximation.^{69–71} The calculations were performed in a vacuum and in solvent using the continuum conductor-like screening (COSMO) model,⁷² as implemented

- (60) Booth, B. L.; Haszeldine, R. N.; Laali, K. *J. Chem. Soc., Perkin Trans. 1980*, *1*, 2887.
(61) (a) Franken, A.; King, B. T.; Rudolph, J.; Rao, P.; Noll, B. C.; Michl, J. *Coll. Czech. Chem. Commun.* **2001**, *66*, 1238–1249. (b) Michl, J.; King, B. T.; Janoušek, Z. U.S. Patent No. 5,731,470, March 24, 1998.
(62) Frisch, M. J., et al. Gaussian 03, revision B.02; Gaussian, Inc.: Pittsburgh, PA, 2003.
(63) Molcas: a program package for computational chemistry, version 6.4. Karlström, G.; Lindh, R.; Malmqvist, P.-Å.; Roos, B. O.; Ryde, U.; Veryazov, Widmark, V. P. O.; Cossi, M.; Schimmlerfennig, B.; Neogrady, P.; Seijo, L. *Comput. Mater. Sci.* **2003**, *28*, 222.
(64) Ahlrichs, R.; Bär, M.; Häser, M.; Horn, H.; Kölmel, C. *Chem. Phys. Lett.* **1989**, *162*, 165.
(65) Sierka, M.; Hogeekamp, A.; Ahlrichs, R. *J. Chem. Phys.* **2003**, *118*, 9136.
(66) Becke, A. D. *Phys. Rev. A* **1988**, *38*, 3098.
(67) Perdew, J. P. *Phys. Rev. B* **1986**, *33*, 8822.
(68) Schäfer, A.; Huber, C.; Ahlrichs, R. *J. Chem. Phys.* **1994**, *100*, 5829.
(69) Eichkorn, K.; Treutler, O.; Öhm, H.; Häser, M.; Ahlrichs, R. *Chem. Phys. Lett.* **1995**, *242*, 652.
(70) Eichkorn, K.; Weigend, F.; Treutler, O.; Ahlrichs, R. *Theor. Chem. Acc.* **1997**, *97*, 119.
(71) Weigend, F. *Phys. Chem. Chem. Phys.* **2006**, *8*, 1057.
(72) Klant, A.; Schuurmann, G. *J. Chem. Soc., Perkin Trans.* **1993**, *2*, 799.

in Turbomole 5.7.⁷³ For model solvent calculations we used acetone. Among all solvents for which parameters are available, its dielectric constant ($\epsilon = 20.70$) is the closest to that of the real solvent, liquid SO_2 ($\epsilon = 17.6$).

General Procedures for Cation Exchange. Four techniques were used for exchanging the cation associated with a CB_{11}^- anion. The exchange of the monovalent cations H^+ , Cs^+ , Rb^+ , K^+ , Na^+ , Li^+ , Ag^+ , Tl^+ , NMe_3H^+ , and NMe_4^+ for another cation on the list can be achieved by partitioning an Et_2O solution (or 70/30 Et_2O /acetone for especially hydrophilic salts such as Li^+ **1a**) of less than 10 g/L concentration of the starting cation against an equal volume of a concentrated (10–20% w/w) aqueous solution of the chloride salt of the desired cation. Yields are quantitative when a 3×3 countercurrent extraction is used. The combined product-containing ether phases are evaporated to dryness and the product is dissolved in Et_2O (or 70/30 Et_2O /acetone), leaving the insoluble chloride salts behind. This method fails for very lipophilic cations such as PPh_4^+ . For Li^+ , this method produces a mixture of Li^+ and H_3O^+ salts, which is unstable above 100 °C. To avoid decomposition upon drying, the mixture needs to be neutralized with LiOH .

The most general method for cation exchange, but most time-consuming, is using a strongly acidic methanolic ion exchange column (Amberlyst XN-1010) in the H_3O^+ form. A methanol solution of the starting cation, up to 10 g/L, is allowed to slowly run through a column containing a 50-fold molar excess of the resin. The methanolic solution of the free acid can be neutralized with the basic oxide or hydroxide of the desired cation. A third method is the precipitation of an insoluble salt of a cation, such as PPh_4^+ , from a methanolic solution of a soluble salt of a cation, such as Cs^+ . Alternatively, the NMe_4^+ or NMe_3H^+ salt can be precipitated from an aqueous solution of the hydrated free acid or other water soluble salt. The fourth method is the metathesis of the Ag^+ or Tl^+ salts with the chloride of the desired cation.

Cyclic Voltammetry. Electrochemical measurements were performed using an SO_2 manifold equipped with three platinum electrodes. The working electrode was a disk with a surface area of $\sim 0.2 \text{ mm}^2$ (**3a**, **4a**, **7a**, **8a**, **10a**, **11a**, **12a**, **13a**, **14a**) or a 0.5 mm diameter wire with an area of $\sim 40 \text{ mm}^2$ (**1a**, **2a**, **5a**, **6a**, **9a**, **15a**, **16a**). The auxiliary electrode was a 12 cm tightly coiled wire, and the reference electrode was a 2.5 cm wire. Oxidation potentials were referenced to the ferrocene/ferricenium couple. Typical ferrocene peak splittings were 50–150 mV. Approximate current densities are shown in Figure 1. The volume of the conical electrochemical cell was 2 mL. SO_2 was stored in a reservoir over P_2O_5 and then distilled onto a mixture of the dry analyte, ferrocene, and supporting electrolyte ($\text{Bu}_4\text{N}^+\text{PF}_6^-$). The concentrations were about 10 or 20 mM for the cesium carborate salt, $\sim 3 \text{ mM}$ for ferrocene, and $\sim 100 \text{ mM}$ for the electrolyte. Measurements were carried out at 0 °C with a BAS-CW50 instrument at a scan rate of 0.5 V/s. An increase to 1 V/s had no appreciable effect. The first scans were used to obtain results since electrode fouling was observed for some of the anions that gave irreversible waves.

Tetramethylammonium 1-Methylcarba-closo-dodecaborate, [Me₄N][1-MeCB₁₁H₁₁] (2a**):** $\text{Me}_3\text{NH}^+\text{1a}$ (7.0 g, 34.5 mmol) was placed in a 250 mL Schlenk flask and dried under vacuum at 100 °C for 60 min. The flask was charged with argon, and THF (150 mL, freshly distilled from Na/benzophenone) was added. A 1.6 M solution of $n\text{-BuLi}$ in hexanes (86.25 mL, 138 mmol) was added dropwise over 60 min at 0 °C. The solution was allowed to warm to room temperature and stirred an additional 60 min. Methyl iodide (8.6 mL, 138 mmol) was added, and the mixture was stirred for an additional 30 min. Water (25 mL) was added, and the reaction mixture evaporated to dryness. The residue was extracted with diethyl ether ($3 \times 100 \text{ mL}$), and the solution was washed with a 20% solution of CsCl ($3 \times 50 \text{ mL}$). The combined CsCl wash was extracted with diethyl ether ($3 \times 50 \text{ mL}$). The combined

organic phase was evaporated to dryness, and the crude solid recrystallized from a minimum amount of water. Yield: 6.88 g (92%). For $\text{N}(\text{CH}_3)_4^+$ salt: $^1\text{H}\{^{11}\text{B}\}\text{NMR}$ δ 3.42 [s, 12H, $\text{N}(\text{CH}_3)_4^+$], 1.74 [s, 5H, BH], 1.54 [s, 5H, BH], 1.50 [s, 3H, $\text{CH}_3(1)$], 1.46 [s, 1H, BH(12)]. $^{11}\text{B}\{^1\text{H}\}\text{NMR}$ δ -11.09 [s, 1B, B(12)], -12.83 [s, 10B, B(2–11)]. $^{13}\text{C}\{^1\text{H}\}\text{NMR}$ δ 55.84 [t, $\text{N}(\text{CH}_3)_4$], 27.68 [s, $\text{CH}_3(1)$]; IR (KBr pellet) 2938, 2875, 2544, 1458, 1311, 1194, 1039, 938, 728, 487 cm^{-1} . MS ESI(-) m/z 157, expected isotopic distribution. For PPh_4^+ salt: Anal. Calcd for $\text{C}_{26}\text{B}_{11}\text{H}_{34}\text{P}$: C, 62.91; H, 6.90. Found: C, 63.20; H, 6.84.

Cesium 2,3,4,5,6-Pentamethylcarba-closo-dodecaborate, [Cs][(2–6)-Me₅CB₁₁H₇] (3a**):** Sodium (0.5 g) was dissolved in a neck of liquid ammonia (20 mL) and dry THF (5 mL) in a three-neck round-bottom flask equipped with a PTFE-clad stir bar. Methanol (200 μL) was added to the ammonia. $\text{Cs}^+\text{35a}^{74}$ (0.30 g, 0.27 mmol) was added, and the mixture was stirred at -78 °C for 30 min at which point the NH_3 was evaporated. Et_2O was added to the flask, and the remaining sodium was then carefully quenched at -78 °C with methanol. The solvents were evaporated, and the remaining solids were washed with Et_2O ($3 \times 50 \text{ mL}$). The combined ethereal solution was partitioned with a 20% aqueous solution of CsCl ($3 \times 50 \text{ mL}$). The CsCl solution was then washed with Et_2O ($3 \times 50 \text{ mL}$). The ethereal solutions were combined and evaporated to dryness. The resulting solid was purified by column chromatography using reversed phase C_{18} silica gel with a 50/50 methanol/water eluent. Product containing fractions were combined, and the methanol was evaporated on a rotary evaporator. The resulting aqueous solution was extracted with Et_2O ($3 \times 50 \text{ mL}$), and then the Et_2O layer was partitioned against a 20% aqueous CsCl solution ($3 \times 50 \text{ mL}$). The organic solution was evaporated to dryness, the remaining solids were triturated with Et_2O , and the filtered organic solution was evaporated to dryness to provide $\text{Cs}^+\text{3a}$. Yield: 80 mg (80%). For Cs^+ salt: $^1\text{H}\{^{11}\text{B}\}\text{NMR}$ δ 0.110 [s, 15H, BCH_3], 1.37 [s, 5H, BH], 1.21 [s, 1H, BH], 1.205 [s, 1H, CH(1)]. $^1\text{H}\{^{13}\text{C}\}\{^{11}\text{B}\}$ gHMBC δ 68.19 [s, C(1)]. $^{11}\text{B}\{^1\text{H}\}$ NMR δ -8.36 [s, 5B, B(2–6)], -10.608 [s, 1B, B(12)], -14.173 [(s, 5B, B(7–11))]. IR (KBr) 2942, 2899, 2831, 2490, 1616, 1435, 1313, 1180, 1037, 1008, 877, 802, 470 cm^{-1} . ESIMS (-) m/z 213, expected isotopic distribution. For PPh_4^+ salt: Anal. Calcd for $\text{C}_{30}\text{H}_{42}\text{B}_{11}\text{P}$: C, 65.21, H, 7.66. Found: C, 65.05; H, 7.57.

Cesium 7,8,9,10,11-Pentamethylcarba-closo-dodecaborate, [Cs][(7–11)-Me₅CB₁₁H₇] (4a**):** $\text{Bu}_4\text{N}^+\text{24a}$ (0.67 g, 1.03 mmol) was dissolved in THF (3 mL) and then added dropwise to a solution of Na ($\sim 1 \text{ g}$) in THF (40 mL), NH_3 (40 mL), and methanol (100 μL) at -40 °C. Care was taken to ensure that a deep blue color persisted throughout the reaction. After the addition was complete, the reaction mixture was stirred for 5 min and then quenched with methanol, followed by water. The ammonia was allowed to evaporate slowly, and then water was added to the remaining slurry. The aqueous solution was extracted with ether ($3 \times 50 \text{ mL}$), and the ether layers were combined. Water (150 mL) was added, and the ether was evaporated. The aqueous solution was filtered and extracted one more time with ether and then washed with a 10% aqueous solution of CsCl . The ether was removed, leaving a white solid. Yield: 67 mg (63%). For PPh_4^+ salt: $^1\text{H}\{^{11}\text{B}\}$ NMR δ 7.92 [t, 4H, PPh_4^+], 7.76 [m, 8H, PPh_4^+], 7.60 [m, 8H, PPh_4^+], 1.89 [s, 1H, CH(1)], 1.28 [s, 5H, BH(2–6)], 1.21 [s, 1H, BH(12)], -0.005 [s, 15H, $\text{CH}_3(7–11)$]. $^1\text{H}\{^{13}\text{C}\}\{^{11}\text{B}\}$ gHMBC δ 136.17 [d, PPh_4^+], 134.53 [d, PPh_4^+], 130.07 [d, PPh_4^+], 117.50 [d, PPh_4^+], 43.32 [s, C(1)], -0.20 [s, $\text{CH}_3(7–11)$]. ^{11}B NMR δ -1.25 [d, 1B, B(12)], -6.49 [s, 5B, B(7–11)], -19.55 [d, 5B, B(2–6)]. IR (KBr pellet) 3433, 2920, 2532, 2354, 1635, 1052 cm^{-1} . ESI MS(-) m/z 213, expected isotope distribution. Anal. Calcd for $\text{C}_{30}\text{H}_{42}\text{B}_{11}\text{P}$: C, 64.95; H, 7.64. Found: C, 64.80; H, 7.62.

Tetramethylammonium 12-Methylcarba-closo-dodecaborate, [Me₄N][12-MeCB₁₁H₁₁] (5a**):** The compound was synthesized according to a literature procedure.¹⁴

(73) Schäfer, A.; Klamt, A.; Sattel, D.; Lohrenz, J. C. W.; Eckert, F. *Phys. Chem. Chem. Phys.* **2000**, *2*, 2187.

(74) Stasko, D.; Reed, C. A. *J. Am. Chem. Soc.* **2002**, *124*, 1148.

Cesium 1,2,3,4,5,6-Hexamethylcarba-closo-dodecaborate, [Cs][(1-6)-Me₆CB₁₁H₆] (6a): A 50% pure sample of Cs⁺28a (497 mg, principal impurities Cs⁺Me_(6-n)I_(6+n)CB₁₁⁻, *n* = +1, -1) was dissolved in NH₃ at -78 °C. Metallic sodium (200 mg) was added, and the mixture was refluxed for 2 h; afterwards, *i*-PrOH (500 μL) was added, and the NH₃ was evaporated. Et₂O was added to the flask, and the remaining sodium carefully quenched with MeOH. The ethereal solution was brought to a total volume of 100 mL and then partitioned against a 20% aqueous CsCl solution (3 × 20 mL). The organic layer was evaporated to dryness, the solids were triturated with Et₂O, and the filtered solution was taken to dryness. The resulting product was purified by preparative HPLC (25 mm × 100 mm, isocratic 70/30 MeOH/water with 1% AcOH and 0.7% Et₃N, evaporative light scattering detection). Product containing fractions were combined, and MeOH was removed on a rotary evaporator. The resulting aqueous solution was extracted with Et₂O (100 mL), and then the Et₂O layer was partitioned against 20% aqueous CsCl (3 × 20 mL). The organic layer was evaporated to dryness, the solids were triturated with Et₂O, and the filtered organic solution was evaporated to dryness. Yield: 80 mg (80%) based on starting material purity. Analytically pure material was recrystallized from hot water. For Cs⁺ salt: ¹H{¹¹B}NMR δ 1.48 [s, 1H, BH(12)], 1.33 [s, 5H, BH(7-11)], 0.74 [s, 3H, CH₃(1)], -0.06 [s, 15H, BCH₃(2-6)]. ¹³C{¹¹B}NMR δ 13.62 [s, CH₃(1)], -0.26 [s, CH₃(2-6)]. ¹¹B NMR δ -7.73 [s, 5B, B(2-6)], -10.95 [d, 1B, 139, B(12)], -14.66 [d, 5B, 129, B(7-11)]. IR (KBr) 2935, 2903, 2501, 1632, 1437, 1377, 1306, 1138, 1008, 866 cm⁻¹. ESI MS(-) *m/z* 227. Anal. Calcd for C₇H₂₄B₁₁Cs: C, 23.35; H, 6.72. Found: C, 23.92; H, 7.16.

Cesium 1,7,8,9,10,11-Hexamethylcarba-closo-dodecaborate, [Cs][1,(7-11)-Me₆CB₁₁H₆] (7a): NBu₄⁺24a (0.146 g, 0.251 mmol) was dissolved in 1,2-dimethoxyethane (6 mL) in a sealable glass vessel equipped with a PTFE-clad magnetic stir bar, and iodine monochloride (0.5 g, 3.01 mmol) was added. The vessel was sealed and heated to 130 °C in a microwave oven for 30 min. After cooling to room temperature the reaction mixture was a colorless clear solution. The solvent was removed under reduced pressure, and water and ether were added. The aqueous layer was extracted with Et₂O (3 × 50 mL). The ethereal solutions were combined, and the solvent was removed under reduced pressure. Addition of water (10 mL) to the orange solution afforded a yellow precipitate. The precipitate was collected by filtration and recrystallized to give NBu₄⁺34a. Yield: 102 mg, mixture of compounds containing three and four iodines in the anion (49%, based on main product with 3 iodines). The product was used without further purification. ESI MS(-) *m/z* 590 and 716, expected isotopic distribution. Cs⁺34a (0.102 g) was dissolved in freshly distilled THF (10 mL) and cooled to 0 °C. A solution of *n*-BuLi (2 mL, 3.2 mmol, 1.6 M in hexanes) was added slowly, and stirring was continued for an additional 30 min. Methyl iodide (1.14 g, 8.0 mmol) was added, and the mixture was allowed to warm up to rt. Stirring was continued overnight. The reaction was quenched with water (20 mL), and the organic layer was separated. The aqueous layer was extracted with Et₂O (3 × 50 mL). The combined organic solutions were washed with a 20% aqueous CsCl solution (3 × 50 mL). The combined CsCl wash was extracted with Et₂O (3 × 50 mL), and all ethereal solutions were pooled and evaporated on a rotary evaporator. The remaining solid was triturated with Et₂O and filtered. The Et₂O was evaporated to give Cs⁺26a. Yield: 69 mg (76%, based on main product with three iodines). The product was used without further purification. ESI MS(-) *m/z* 604 and 731, expected isotopic distribution. Cs⁺26a (66 mg, mixture of [(2-6,12)-I_x-(1,7-11)-Me₆CB₁₁]⁻, *x* = 2, 3) was dissolved in THF and added to a solution of Na (100 mg) in THF (4 mL), NH₃ (4 mL), and MeOH (10 μL) at -40 °C. After the addition of the borate(-) solution, stirring was continued for 15 min, and then MeOH (2 mL) was added. The ammonia was allowed to evaporate slowly, and then water was added. The resulting solution was extracted with Et₂O (3 × 50 mL). The combined ethereal layers were washed with 20% CsCl

solution. The organic layer was evaporated to dryness, the solids were triturated with Et₂O, and the filtered solution was taken to dryness. Crude yield: 24 mg (66%). The product was purified by HPLC (reversed phase C₁₈ column, 45% methanol, 55% water). For PPh₄⁺ salt: ¹H{¹¹B}NMR δ 8.02 [m, 8H, PPh₄⁺], 7.87 [m, 12H, PPh₄⁺], 1.47 [s, 5H, BH(2-6)], 1.40 [s, 3H, CH₃(1)], 1.78 [s, 1H, BH(12)]. ¹H{¹³C} {¹¹B} gHMQC δ 136.24 [s, PC₆H₅], 135.50 [s, PC₆H₅], 131.32 [s, PC₆H₅], 118.7 [s, PC₆H₅], 53.5 [s, C(CH₃)], -9.45 [s, CH₃(7-11)]. ¹H{¹³C} {¹¹B} gHMBC δ 56.18 [s, C(1)]. ¹¹B NMR δ -5.17 [s, 6B, B(7-12)], -14.63 [d, 5B, B(2-6)]. For Cs⁺ salt: IR (KBr) 2935, 2903, 2501, 1632, 1437, 1377, 1306, 1138, 1008, 866 cm⁻¹. ESI MS(-) *m/z* 227. Anal. Calcd for C₃₁H₄₄B₁₁P: C, 65.72; H, 7.83. Found: C, 66.00; H, 7.81.

Tetramethylammonium 1,12-Dimethylcarba-closo-dodecaborate, [Me₄N][1,12-Me₂CB₁₁H₁₀] (8a): The compound was synthesized according to a literature procedure.¹⁴

Tetraphenylphosphonium 2,3,4,5,6,7,8,9,10,11-Decamethylcarba-closo-dodecaborate, [PPh₄][(2-11)-Me₁₀CB₁₁H₂] (9a): Cs⁺36a (1.00 g, 1.34 mmol) was reduced as described for the preparation of 3a. Yield: 0.58 g (70%). For PPh₄⁺ salt: ¹H{¹¹B}NMR δ 7.92 [t, 4H, PPh₄⁺], 7.76 [m, 8H, PPh₄⁺], 7.60 [m, 8H, PPh₄⁺], 1.31 [s, 1H, BH(12)], 1.28 [s, 1H, CH(1)], -0.18 [s, 15H, BCH₃(2-6)], -0.25 [s, 15H, BCH₃(7-11)]. ¹H{¹³C}NMR δ 118.82 [d, PPh₄⁺], 131.37 [d, PPh₄⁺], 135.63 [d, PPh₄⁺], 62.43 [s, C(1)], -1.50 [s, CH₃(2-6)], -1.68 [s, CH₃(7-11)]. ¹¹B NMR δ -2.46 [s, 1B, B(12)], -8.81 [s, 5B, B(7-11)], -11.74 [s, 5B, B(2-6)]. For Cs⁺ salt: IR (KBr pellet) 2928, 2893, 2829, 2530, 2448, 1438, 1306, 1081, 1038 cm⁻¹. ESI MS(-) *m/z* 283, expected isotopic distribution. For PPh₄⁺ salt: Anal. Calcd for C₃₅H₅₂B₁₁P: C, 67.51; H, 8.42. Found: C, 67.44; H, 8.51.

Cesium 2,3,4,5,6,12-Hexamethylcarba-closo-dodecaborate, [Cs][(2-6),12-Me₆CB₁₁H₆] (10a): Cs⁺21a (0.248 g, 0.25 mmol) was dissolved in THF (5 mL) and was added dropwise slowly to a solution of Na (0.5 g) in a mixture of THF (20 mL), NH₃ (20 mL), and methanol (150 μL) at -40 °C. Care was taken to ensure that a deep blue color persisted throughout the reaction. After the addition was complete, the reaction mixture was stirred for 5 min and then quenched with methanol, followed by water. The ammonia was allowed to evaporate slowly, and then water was added to the remaining slurry. The aqueous solution was extracted with ether (3 × 50 mL) and then washed three times with a 10% aqueous solution of CsCl. The ether was evaporated to give off-white crystals. Yield: 0.067 g (74.4%). For PPh₄⁺ salt: ¹H{¹¹B}NMR δ 7.91 [t, 4H, PPh₄⁺], 7.78 [m, 8H, PPh₄⁺], 7.61 [m, 8H, PPh₄⁺], 1.21 [s, 5H, BH(7-11)], 1.06 [s, 1H, CH(1)], 0.07 [s, 15H, BCH₃(2-6)], -0.172 [s, 3H, BCH₃(12)]. ¹³C{¹¹B}NMR δ 136.06 [d, PPh₄⁺], 134.56 [d, PPh₄⁺], 131.07 [d, PPh₄⁺], 1H{¹³C} {¹¹B} gHMQC δ 61.95 [s, C(1)], 29.88 [s, PPh₄⁺], 0.33 [s, CH₃(2-6,12)]. ¹¹B NMR δ -3.49 [s, 1B, B(12)], -9.28 [s, 5B, B(2-6)], -13.93 [d, 5B, B(7-11)]. IR (KBr pellet) 3437, 2931, 2899, 2826, 2499, 2357, 1635, 1436, 1313, 1179, 1031, 1003, 877, 673 cm⁻¹. ESI MS(-) *m/z* 227, expected isotopic distribution. For PPh₄⁺ salt: Anal. Calcd for C₃₁H₄₄B₁₁P: C, 65.72; H, 7.83. Found: C, 65.95; H, 7.62.

Cesium 7,8,9,10,11,12-Hexamethylcarba-closo-dodecaborate, [Cs][(7-12)-Me₆CB₁₁H₆] (11a): Cs⁺29a (563 mg, 1.09 mmol) was dissolved in sulfolane (20 mL) in a round-bottom flask equipped with a reflux condenser, and the system was put under an Ar atmosphere. CsF (250 mg) was added, and the reaction mixture was heated to 225 °C using a Wood's metal bath. After 4 h, additional CsF (1.5 g) was added and the reaction mixture was heated to 270 °C. After an additional 3 h, more CsF (500 mg) was added and the reaction mixture was heated an additional 12 h at 270 °C. The reaction mixture was poured into water (100 mL) and extracted with Et₂O (2 × 50 mL). The combined ether layers were partitioned against a 20% aqueous CsCl solution (50 mL, countercurrent, 2 × 2). The ethereal phase was evaporated to dryness, and the resulting solid was triturated with Et₂O. The filtered ether was evaporated to dryness, and the residue was recrystallized from hot water. Yield: 292 mg (75%).

A second recrystallization afforded analytically pure material. For Cs^+ salt: $^1\text{H}\{^{11}\text{B}\}$ NMR δ 1.83 [s, 1H, CH(1)], 1.34 [s, 5H, BH(2–6)], –0.16 [s, 15H, $\text{BCH}_3(7–11)$], –0.52 [s, 3H, $\text{BCH}_3(12)$]. $^{13}\text{C}\{^{11}\text{B}\}$ NMR δ 42.14 [s, C(1)], –1.51 [s, $\text{BCH}_3(7–11)$], –2.32 [s, $\text{BCH}_3(12)$]. ^{11}B NMR δ 1.80 [s, 1B, B(12)], –6.05 [s, 5B, B(7–11)], –19.24 [d, 5B, B(2–6)]. IR (KBr) 2919, 2892, 2827, 2533, 2468, 1301, 1143, 1095, 1002, 970, 877 cm^{-1} . ESI MS(–) m/z 227, expected isotopic distribution. Anal. Calcd for $\text{C}_7\text{H}_{24}\text{B}_{11}\text{Cs}$: C, 23.35; H, 6.72. Found: C, 23.67; H, 6.96.

Tetraphenylphosphonium 2,3,4,5,6,7,8,9,10,11,12-Undecamethylcarba-closo-dodecaborate, $[\text{PPh}_4][(-12)\text{-Me}_{11}\text{CB}_{11}\text{H}_2]$ (12a): $\text{Et}_3\text{-NH}^+\mathbf{1a}$ (0.74 g, 3 mmol) was methylated as described for the preparation of **16a** and isolated as the PPh_4^+ salt. Yield: 1.15 g (60%). For PPh_4^+ salt: $^1\text{H}\{^{11}\text{B}\}$ NMR δ 7.92 [t, 4H, PPh_4^+], 7.76 [m, 8H, PPh_4^+], 7.60 [m, 8H, PPh_4^+], 1.07 [s, 15H, $\text{CH}_3(1)$], –0.19 [s, 15H, $\text{BCH}_3(7–11)$], –0.42 [s, 15H, $\text{BCH}_3(2–6)$], –0.53 [s, 3H, $\text{BCH}_3(12)$]. $^{13}\text{C}\{^1\text{H}\}$ NMR δ 135.63 [d, PPh_4^+], 131.37 [d, PPh_4^+], 118.82 [d, PPh_4^+], 61.13 [s, C(1)], –3.67 [s, $\text{CH}_3(2–6)$], –2.43 [s, $\text{CH}_3(12)$]. ^{11}B NMR δ –0.60 [s, 1B, B(12)], –8.71 [s, 5B, B(7–11)], –12.07 [s, 5B, B(2–6)]. For Cs^+ salt: IR (KBr pellet) 2896, 2814, 1431, 1378, 1302, 1179, 908 cm^{-1} . ESI MS(–) m/z 297, expected isotopic distribution. For PPh_4^+ salt: Anal. Calcd for $\text{C}_{35}\text{H}_{52}\text{B}_{11}\text{P}$: C, 67.51; H, 8.42. Found: C, 67.56; H, 8.42.

Cesium 1,7,8,9,10,11,12-Heptamethylcarba-closo-dodecaborate, $[\text{Cs}][1,(7–12)\text{-Me}_7\text{CB}_{11}\text{H}_5]$ (13a): Sodium (0.5 g) was dissolved in a mixture of liquid ammonia (20 mL) and anhydrous THF (5 mL) in a three-neck round-bottom flask equipped with a PTFE-clad stir bar. Methanol (200 μL) was added to the NH_3 . $\text{Cs}^+\mathbf{33a}$ (0.15 g, 0.15 mmol) was added, and the mixture was stirred at -78°C for 30 min after which the NH_3 was evaporated. Et_2O was added to the flask, and the remaining sodium was then carefully quenched at -78°C with methanol. The solvents were evaporated, and the remaining solids were washed with Et_2O (3×50 mL). The combined ethereal solution was partitioned with a 20% aqueous solution of CsCl (3×50 mL). The CsCl solution was then washed with Et_2O (3×50 mL). The ethereal solutions were combined and evaporated to dryness. The resulting solid was purified by column chromatography using reversed phase C_{18} silica gel with a 50/50 methanol/water eluent. Product containing fractions were combined, and the methanol was evaporated on a rotary evaporator. The resulting aqueous solution was washed with Et_2O (3×50 mL), and then the Et_2O layer was partitioned against a 20% aqueous CsCl solution (3×50 mL). The organic layer was evaporated to dryness, the remaining solids were triturated with Et_2O , and the filtered organic solution was evaporated to dryness to provide $\text{Cs}^+\mathbf{13a}$. Yield: 80 mg (80%). For Cs^+ salt: $^1\text{H}\{^{11}\text{B}\}$ NMR δ –0.58 (s, 3H, BCH_3), –0.17 (s, 15H, BCH_3), 1.46 [s, 3H, $\text{CH}_3(1)$], 1.48 [s, 5H, BH(2–6)]. $^1\text{H}\{^{13}\text{C}\}$ $\{^{11}\text{B}\}$ gHMBC δ –3.20 [s, $\text{CH}_3(12)$], –1.42 [s, $\text{CH}_3(7–11)$], 26.02 [s, $\text{CH}_3(1)$]. $^1\text{H}\{^{13}\text{C}\}$ $\{^{11}\text{B}\}$ gHMBC δ 55.70 [s, C(1)]. $^{11}\text{B}\{^1\text{H}\}$ NMR δ –15.03 [s, 5B, B(2–6)], –5.50 [s, 5B, B(7–11)], –2.86 [s, 1B, B(12)]. IR (KBr) 2928, 2893, 2828, 2522, 2363, 2335, 1437, 1384, 1305, 1261, 1077, 901, 801, 464, 425 cm^{-1} . ESI MS(–) m/z 241, expected isotopic distribution. For PPh_4^+ salt: Anal. Calcd for $\text{C}_{32}\text{H}_{46}\text{B}_{11}\text{P}$: C, 66.20, H, 7.99. Found: C, 66.11; H, 7.91.

Cesium 1,2,3,4,5,6,12-Heptamethylcarba-closo-dodecaborate, $[\text{Cs}][1(–6),12\text{-Me}_7\text{CB}_{11}\text{H}_5]$ (14a): $\text{Cs}^+\mathbf{32a}$ (0.681 g, 1.9 mmol) was dissolved in THF (10 mL). It was added dropwise slowly to a solution of K (1 g, 25.5 mmol) in a mixture of THF (30 mL), NH_3 (30 mL), and methanol (150 μL) at -40°C . Care was taken to ensure that a deep blue color persisted throughout the reaction. After the addition was complete, the reaction was stirred for 5 min and then quenched with methanol, followed by water. The ammonia was allowed to evaporate slowly, and then water was added to the remaining slurry. The aqueous solution was extracted with ether (3×50 mL) and then washed three times with a 10% aqueous solution of CsCl . The ether was evaporated to give a white solid. Yield: 154 mg (44%). For PPh_4^+ salt: $^1\text{H}\{^{11}\text{B}\}$ NMR δ 7.91 [t, 4H, PPh_4^+], 7.78 [m, 8H, PPh_4^+], 7.61 [m, 8H, PPh_4^+],

1.28 [s, 5H, BH(7–11)], 0.74 [s, 3H, $\text{CH}_3(1)$], 0.07 [s, 18H, $\text{BCH}_3(2–6,12)$]. $^1\text{H}\{^{13}\text{C}\}$ $\{^{11}\text{B}\}$ gHMBC δ 134.60 [s, PPh_4^+], 131.43 [s, PPh_4^+], 10.27 [s, $\text{CH}_3(1)$], –0.71 [s, $\text{CH}_3(2–6,12)$]. $^1\text{H}\{^{13}\text{C}\}$ $\{^{11}\text{B}\}$ gHMBC δ 57.41 [s, C(1)]. ^{11}B NMR δ –2.43 [s, 1B, B(12)], –7.13 [d, 5B, B(2–6)], –13.10 [d, 5B, B(7–11)]. IR (KBr pellet) 3412, 2935, 2903, 2830, 2524, 2450, 1648, 1431, 1313, 1137, 1007, 979, 877, 669, 567 cm^{-1} . ESI MS(–) m/z 241, expected isotopic distribution. For PPh_4^+ salt: Anal. Calcd for $\text{C}_{32}\text{H}_{46}\text{B}_{11}\text{P}$: C, 66.20; H, 7.99. Found: C, 65.95; H, 7.62.

Tetraphenylphosphonium 1,2,3,4,5,6,7,8,9,10,11-Undecamethylcarba-closo-dodecaborate, $[\text{PPh}_4][1(–11)\text{-Me}_{11}\text{CB}_{11}\text{H}]$ (15a): $\text{PPh}_4^+\mathbf{37a}$ (1.00 g, 1.31 mmol) was reduced as described for **3a**. Yield: 830 mg (93%). For Cs^+ salt: $^1\text{H}\{^{11}\text{B}\}$ NMR δ 1.31 [s, 1H, BH(12)], 0.81 [s, 3H, $\text{CH}_3(1)$], –0.21 [s, 15H, $\text{BCH}_3(7–11)$], –0.26 [s, 15H, $\text{BCH}_3(2–6)$]. For PPh_4^+ salt: $^{13}\text{C}\{^1\text{H}\}$ NMR δ 136.29 [d, PPh_4^+], 135.58 [d, PPh_4^+], 118.85 [d, PPh_4^+], 58.20 [s, C(1)], 13.00 [s, $\text{CH}_3(1)$], –1.73 [s, $\text{CH}_3(7–11)$], –3.41 [s, $\text{CH}_3(2–6)$]. ^{11}B NMR δ –2.39 [s, 1B, B(12)], –8.82 [s, 5B, B(7–11)], –10.48 [s, 5B, B(2–6)]. For Cs^+ salt: IR (KBr pellet) 2925, 2887, 2823, 2443, 1434, 1304, 1110, 921 cm^{-1} . ESI MS(–) m/z 297, expected isotopic distribution. For PPh_4^+ salt: Anal. Calcd for $\text{C}_{36}\text{H}_{54}\text{B}_{11}\text{P}$: C, 67.91; H, 8.55. Found: C, 67.96; H, 8.34.

Tetramethylammonium Dodecamethylcarba-closo-dodecaborate, $[\text{Me}_4\text{N}][\text{CB}_{11}\text{Me}_{12}]$ (16a). Calcium hydride (8.4 g, 200 mmol) was added to a solution of $\text{Cs}^+\mathbf{2a}$ (1.45 g, 5 mmol) in sulfolane (19 mL, 24 g, 200 mmol, freshly distilled under reduced pressure from CaH_2) in a 250 mL, three-necked, round-bottom flask, and the system was placed under argon. The mixture was stirred at 25°C , and methyl triflate (11.3 mL, 16.4 g, 100 mmol) was added to the flask with a syringe pump over a period of 20 h. The stirring was continued for 3 days, after which the reaction mixture solidified. A solution of methyl triflate (5.5 mL) in sulfolane (10 mL) was added to the reaction mixture in one portion and stirring was continued for 2 days, after which the reaction was complete. The solidified reaction mixture was diluted with anhydrous methylene chloride (300 mL), and the solids were removed by vacuum filtration. The filtrate was quenched slowly with 27% ammonium hydroxide (100 mL) solution and extracted with diethyl ether (3×150 mL). The filtered solids were carefully dissolved in 15% HCl (100 mL), and the solution was neutralized with ammonium hydroxide and extracted with diethyl ether (3×50 mL). The combined organic layer was washed with 20% aqueous CsCl (3×50 mL). The combined CsCl wash was extracted with diethyl ether (3×50 mL). The combined ether solution was evaporated. The residual sulfolane was removed by a short path vacuum distillation at 150°C (<0.05 mmHg). The white solid collected is $\text{Cs}^+\mathbf{16a}$ (2.0 g, 90% yield, 99% pure by HPLC). Recrystallization from water afforded analytically pure material. For Cs^+ salt: ^1H NMR δ 0.80 [s, 3H, $\text{CH}_3(1)$], –0.33 [s, 15H, $\text{BCH}_3(2–6)$], –0.40 [s, 15H, $\text{BCH}_3(7–11)$], –0.51 [s, 3H, $\text{BCH}_3(12)$]. $^{13}\text{C}\{^1\text{H}\}$ NMR δ –3.00 [$\text{CH}_3(2–12)$], 13.31 [s, $\text{CH}_3(1)$]. ^{11}B NMR δ –0.60 [s, 1B, B(12)], –8.67 [s, 5B, (7–11)], –10.70 [s, 5B, (2–6)]. For Cs^+ salt: IR (KBr pellet) 2928, 2893, 2827, 1438, 1304, 1150, 913 cm^{-1} , Raman (powder) 2903, 2831, 458, 433, 418 cm^{-1} . ESI MS(–) m/z 311, expected isotopic distribution. For PPh_4^+ salt: Anal. Calcd for $\text{C}_{37}\text{B}_{11}\text{H}_{56}\text{P}$: C, 68.29; H, 8.67. Found: C, 68.15; H, 8.74.

Cesium 1-Triisopropylsilylcarba-closo-dodecaborate, $[\text{Cs}][1(-i\text{-Pr})_3\text{SiCB}_{11}\text{H}_{11}]$ (18a): $\text{NMe}_3\text{H}^+\mathbf{1a}$ (2.00 g, 9.85 mmol) was added to a 250 mL round-bottom flask equipped with a PTFE-clad magnetic stir bar and a septum. After filling the system with Ar, freshly distilled THF (100 mL) was added. $n\text{-BuLi}$ (18.7 mL, 30 mmol, 1.6 M in hexanes) was added slowly over 30 min. After another 60 min, ($i\text{-Pr}$) $_3\text{SiCl}$ (6.4 mL, 30 mmol) was added dropwise over 10 min. After quenching with water (10 mL), the reaction mixture was evaporated to dryness. The residue was dissolved in Et_2O (100 mL) and water (100 mL), and the phases were shaken together. The ether layer was partitioned against 20% aqueous CsCl (2×100 mL), and all aqueous

layers were washed with the same portion of Et₂O (100 mL). The combined organic pool was evaporated to dryness on a rotary evaporator. The solids were triturated with hot benzene, dissolving the product but not the starting material. The starting material was recovered by dissolving with acetone (568 mg). The benzene was removed on a rotary evaporator, and the residue was dissolved in boiling water, adding NH₄OH as necessary to maintain neutral pH (HCl is generated by hydrolysis of residual (*i*-Pr)₃SiCl). The hot solution is quickly filtered through a plug of glass wool and then allowed to cool to 0 °C over 3 h. Pure Cs⁺**18a** (2.66 g, 62%, 78% based on recovered starting material) was collected by vacuum filtration. For Cs⁺ salt: ¹H{¹¹B} NMR δ 1.96 [s, 1H, BH], 1.90 [s, 5H, BH], 1.69 [s, 5H, BH], 1.21–1.29 [m, 3H, CH], 1.15–1.16 [m, 18H, CH₃]. ¹³C{¹H} NMR δ 57.99 [s, C(1)], 20.176 [s, CH₃], 14.128 [s, CH]. ¹¹B{¹H} NMR δ 3.12 [s, 12, B(12)], –11.93 [s, 5B, 150, B(7–11)], –13.76 [s, 5B, 167, B(2–6)] (note: isochronous resonance causes the *J*_{BH} to be overestimated). IR (KBr pellet) 2941, 2914, 2859, 2577, 2539, 2506, 1600, 1464, 1089, 1051, 1013, 883, 726, 660, 638, 611, 503 cm⁻¹. ESI MS(–) *m/z* 299, expected isotopic distribution. Anal. Calcd for C₁₀B₁₁H₃₂SiC_s: C, 27.79; H, 7.46. Found: C, 28.11; H, 7.40.

Cesium 2,3,4,5,6,12-Hexamethyl-7,8,9,10,11-pentaiodocarbocloso-dodecaborate, [Cs][**(2–6)**,**12-Me₆(7–11)-I₅CB₁₁H**] (**21a**): Methyl triflate (5 mL, 26.5 mmol) and triflic acid (1 mL, 3.9 mmol) were added to Cs⁺**30a** (0.495 g, 0.5385 mmol) in a 25 mL round-bottom flask. The reaction flask was capped, and the contents were stirred overnight at 75 °C. The reaction was quenched with methanol (10 mL) followed by a 10% aqueous solution of NaOH (10 mL). Volatiles were removed on a rotary evaporator, and the product was extracted with ether (3 × 50 mL). The combined ether layers were washed three times with a 10% solution of CsCl (50 mL each), and then the ether was removed on a rotary evaporator to give white Cs⁺**21a**. Yield: 0.505 g (95%). For PPh₄⁺ salt: ¹H{¹¹B} NMR δ 7.93 [t, 4H, PPh₄⁺], 7.80 [m, 8H, PPh₄⁺], 7.60 [m, 8H, PPh₄⁺], 2.24 [s, 1H, CH(1)], 0.26 [s, 15H, BCH₃(2–6)], 0.10 [s, 3H, BCH₃(12)]. ¹³C{¹H} NMR δ 136.23 [d, PPh₄⁺], 134.56 [d, PPh₄⁺], 131.44 [d, PPh₄⁺]. ¹H{¹³C} {¹¹B} gHMOC δ 57.56 [s, C(1)], 2.78 [s, CH₃]. ¹¹B NMR δ –1.23 [s, 1B, B(12)], –9.45 [s, 5B, B(2–6)], –16.18 [s, 5B, B(7–11)]. IR (KBr pellet) 3435, 3035, 2588, 1478, 1302, 945, 844, 695, 611 cm⁻¹. ESI MS(–) *m/z* 857, expected isotopic distribution. Anal. Calcd for C₃₁H₃₉B₁₁PI₅: C, 31.13; H, 3.29. Found: C, 30.99; H, 3.08.

Tetramethylammonium 1-Methyl-7,8,9,10,11,12-hexaiodocarbocloso-dodecaborate, [Me₄N⁺][**1-Me-(7–12)-I₆CB₁₁H₅**] (**22a**): The preparation of this anion followed a procedure of Reed and co-workers,⁴⁴ except that the reactant was Me₄N⁺**2a**. Yield: (93%). For Me₄N⁺ salt: ¹H{¹¹B} NMR δ 3.44 [s, 12H, Me₄N⁺], 3.02 [s, 5H, BH(2–6)], 1.56 [s, 3H, CH₃(1)]. ¹³C{¹H} NMR δ 71.33 [s, Me₄N⁺], 56.11 [s, C(1)], 26.07 [s, CH₃(1)]. ¹¹B NMR δ –9.01 [s, 1B, B(12)], –11.45 [s, 5B, B(2–6)], –18.89 [s, 5B, B(7–11)]. For Cs⁺ salt: IR (KBr pellet) 2934, 2690, 2590, 1261, 992, 865, 810, 717, 619 cm⁻¹. ESI MS(–) *m/z* 915, expected isotopic distribution. For PPh₄⁺ salt: Anal. Calcd for C₂₆H₂₈B₁₁I₆P: C, 24.95; H, 2.25. Found: C, 25.09; H, 1.98.

Tetramethylammonium 1-Methyl-12-iodocarbocloso-dodecaborate, [NMe₄][**1-Me-12-ICB₁₁H₁₀**] (**23a**): Me₃NH⁺**2a** (1.10 g, 4.78 mmol) was treated with 4 M HCl (50 mL), and the free acid was extracted with Et₂O (3 × 25 mL). Ether was distilled off, and the residue was dissolved in glacial acetic acid (50 mL). Iodine (0.9 g, 7 mmol) was added, and the reaction mixture was stirred until the ¹¹B NMR spectrum showed only signals of the 1-Me-12-I–CB₁₁H₁₀⁻ anion (3 d). Sodium sulfite (0.3 g) was added, and the solvents were distilled off under reduced pressure. The residue was dissolved in water (50 mL), and NMe₄⁺**23a** was precipitated with 25% aqueous NMe₄OH and then recrystallized from water–methanol. Yield: 1.46 g (86%). For NMe₄⁺ salt: ¹H{¹¹B} NMR δ 3.49 [s, 12H, NMe₄⁺], 1.93 [s, 5H, BH(2–6)], 1.72 [s, 5H, BH(7–11)], 1.35 [s, 3H, CH₃]. ¹³C{¹¹B} NMR δ 62.19 [s, C(1)], 55.87 [s, NMe₄⁺], 26.98 [s, CH₃]. ¹¹B NMR δ –11.38

[d, 5B, 115, B(2–6)], –12.4 [d, 5B, 133, B(7–11)], –19.74 [s, 1B, B(12)]. For Cs⁺ salt: IR (KBr) 2939, 2559, 2530, 1438, 1120, 1022, 940, 813, 725, 680, 543 cm⁻¹. MS FAB *m/z* 285, expected isotopic distribution. For PPh₄⁺ salt: Anal. Calcd for C₂₆H₃₃B₁₁PI: C, 50.18; H, 5.34. Found: 50.34; H, 5.71.

Tetrabutylammonium 7,8,9,10,11-Pentamethyl-12-iodocarbocloso-dodecaborate, [Bu₄N][**(7–11)-Me₅-12-ICB₁₁H₆**] (**24a**): TBAF (1.4 mL, 1 M in THF) was added to Me₄N⁺**31a** (0.170 g, 0.31 mmol) and dissolved in wet DMF (8.5 mL, the reaction will not proceed if solvent and reagents are dry). The reaction mixture was stirred at 75 °C overnight. Solvent and volatiles were removed on a rotary evaporator, and then the off-white solid was washed with H₂O (3 × 50 mL) and dried under vacuum at 80 °C overnight to give Bu₄N⁺**24a**. Yield: 568 mg (91%). For PPh₄⁺ salt: ¹H{¹¹B} NMR δ 7.91 [t, 4H, PPh₄⁺], 7.78 [m, 8H, PPh₄⁺], 7.61 [m, 8H, PPh₄⁺], 2.21 [s, 1H, CH(1)], 1.43 [s, 5H, BH(2–6)], –0.02 [s, 15H, CH₃(7–11)]. ¹H{¹³C} {¹¹B} gHMOC δ 135.85 [s, PPh₄⁺], 134.80 [s, PPh₄⁺], 130.01 [s, PPh₄⁺], 43.44 [s, C(1)], 0.78 [s, CH₃(7–11)]. ¹¹B NMR δ –7.01 [s, 6B, B(7–12)], –20.47 [d, 5B, B(2–6)]. IR (KBr pellet) 3441, 2891, 2528, 1647, 1109, 722, 526 cm⁻¹. ESI MS(–) *m/z* 339, expected isotope distribution. Anal. Calcd for C₃₀H₄₁B₁₁PI: C, 53.11; H, 6.09. Found: C, 53.61; H, 5.95.

Tetramethylammonium 1-Triisopropylsilyl-12-iodocarbocloso-dodecaborate, [Me₄N][**1-*i*-Pr₃Si-12-ICB₁₁H₁₀**] (**25a**): Me₃NH⁺**20a** (1.02 g, 2.04 mmol) was dissolved in 40 mL of THF and cooled to 0 °C. *n*-BuLi (6.2 mL, 0.01 mol) was added dropwise, and the mixture was stirred for 30 min at rt. The solution was cooled again to 0 °C, and triisopropylsilyl chloride (0.7 mL) was added dropwise. The reaction mixture was stirred at rt for 3 h, and the procedure was repeated. After the second treatment, the reaction was complete by ¹¹B NMR. After quenching with H₂O (10 mL), the volatiles were removed on a rotary evaporator. Additional H₂O (50 mL) was added, and a white precipitate formed upon addition of Me₄N⁺Cl⁻. The white solid was filtered and dried at 80 °C overnight. Yield: 1.51 g (98%). For PPh₄⁺ salt: ¹H{¹¹B} NMR δ 7.92 [t, 4H, PPh₄⁺], 7.76 [m, 8H, PPh₄⁺], 7.60 [m, 8H, PPh₄⁺], 2.03 [s, 5H, BH(7–11)], 1.90 [s, 5H, BH(2–6)], 1.08 [m, 21H, (*i*-Pr₃Si)]. ¹³C{¹H} NMR δ 135.85 [d, PPh₄⁺], 134.80 [d, PPh₄⁺], 130.01 [d, PPh₄⁺], 53.23 [s, C(1)], 19.79 [s, CH₃], 13.39 [s, CH]. ¹¹B NMR δ –11.51 [d, 5B, B(7–11)], –14.38 [d, 5B, B(2–6)], –16.10 [s, 1B, B(12)]. ²⁹Si NMR δ 2.93 [s, *i*-Pr₃Si]. IR (KBr pellet) 3430, 2942, 2865, 2534, 2354, 1435, 1110, 993, 882, 720, 691, 522 cm⁻¹. UV–vis (chloroform): λ (ε) 244 (1071), 270 (950), 276 (847). ESI MS (–) *m/z* 424, expected isotopic distribution. For PPh₄⁺ salt: Anal. Calcd for C₃₄H₅₁B₁₁SiPI: C, 53.41; H, 6.72. Found: C, 53.67; H, 6.55.

Cesium 2,3,4,5,6-Pentaiodo-7,8,9,10,11,12-hexamethylcarbocloso-dodecaborate, [Cs][**1-H-(2–6)-I₅CB₁₁Me₆**] (**27a**): Cs⁺**11a** (0.10 g, 0.28 mmol) was dissolved in 1,2-dimethoxyethane (5 mL) in a sealable glass vessel equipped with a PTFE-clad magnetic stir bar, and iodine monochloride (0.5 g, 3.01 mmol) was added. The reaction mixture was sealed, heated to 150 °C, and allowed to stir for 12 h. After cooling to room temperature the reaction mixture was diluted with additional solvent (10 mL) and iodine monochloride was quenched by dropwise addition of a saturated sodium sulfite solution. Addition of water (30 mL) to the pale yellow solution, followed by cooling to 0 °C, afforded a white precipitate. The precipitate was collected by filtration and recrystallized from acetone/water to give Cs⁺**27a**. Yield 151 mg (55%). For Cs⁺ salt: ¹H NMR δ –0.23 (s, 3H, BCH₃), –0.08 (s, 15H, BCH₃), 1.21 (s, 1H, CH). ¹H{¹³C} {¹¹B} gHMOC δ 0.05 [s, B–CH₃(12)], 2.0 [s, B–CH₃(7–11)]. ¹H{¹³C} {¹¹B} gHMBC δ 48.19 [s, C(1)]. ¹¹B NMR: δ –8.36 [s, 5B, B(2–6)], –10.61 [s, 1B, B(12)], –14.17 [s, 5B, B(7–11)]. IR (KBr) 2941, 2897, 2825, 1586, 1482, 1435, 1305, 1261, 1108, 996, 864, 750, 722, 687, 525 cm⁻¹. ESI MS (–) *m/z* 857, expected isotopic distribution. For PPh₄⁺ salt: Anal. Calcd for C₃₁H₃₉B₁₁I₅P: C, 31.13, H, 3.29 Found: C, 30.81; H, 3.31.

Tetraphenylphosphonium 1,2,3,4,5,6-Hexamethyl-7,8,9,10,11,12-Hexaiodocarbocloso-dodecaborate, [PPh₄][(1-6)-Me₆-(7-12)-I₆CB₁₁] (28a): Cs⁺22a (1.00 g, 1.1 mmol) was added to methyl triflate (5 mL, 44.2 mmol) and triflic acid (1.25 mL, 14.1 mmol). The solution was refluxed for 23 h and then diluted with ether (50 mL) and quenched with 26% aqueous ammonium hydroxide (60 mL). The organic layer was separated, washed with an aqueous solution of PPh₄Cl (0.41 g, 1.1 mmol), and concentrated. The resulting solid was recrystallized from methanol. Yield: 0.54 (41%). For PPh₄⁺ salt: ¹H{¹¹B} NMR δ 8.03 [m, 4H, PPh₄⁺], 7.87 [m, 8H, PPh₄⁺], 7.61 [m, 8H, PPh₄⁺], 1.05 [s, 3H, CH₃(1)], 0.15 [s, 15H, CH₃(2-6)]. ¹³C{¹H} NMR δ 136.33 [d, PPh₄⁺], 135.63 [d, PPh₄⁺], 131.37 [d, PPh₄⁺], 118.82 [d, PPh₄⁺], 62.81 [s, C(1)], 17.20 [s, CH₃(1)], 3.62 [s, CH₃(2-6)]. ¹¹B NMR δ -7.83 [s, 1B, B(2-6)], -16.44 [s, 5B, B(7-12)]. IR (KBr pellet) 2996, 2947, 2901, 2845, 1422, 1366, 1328, 1226, 1165, 1335, 1089, 923, 881, 749, 684 cm⁻¹. ESI MS (-) *m/z* 983, expected isotopic distribution. For PPh₄⁺ salt: Anal. Calcd for C₃₁H₃₈B₁₁I₆P: C, 28.17; H, 2.90. Found: C, 27.76; H, 2.86.

Tetramethylammonium 1-Triisopropylsilyl-7,8,9,10,11,12-hexamethylcarba-closo-dodecaborate, [NMe₄][1-(*i*-Pr₃Si)-(7-12)-Me₆CB₁₁H₅] (29a): Cs⁺18a (1.00 g, 2.32 mmol) was combined with CaH₂ (5.0 g, 120 mmol) and sulfolane (25 mL) in a round-bottom flask (100 mL) equipped with a PTFE clad stir bar. MeOTf (3.83 mL, 35 mmol) was added using a syringe pump over 18 h at 10 °C. After 4 days, the mixture was diluted with CH₂Cl₂ (200 mL) and filtered through a coarse frit. The filtrate was quenched with saturated aqueous NH₄OH (20 mL) and then evaporated to dryness using a rotary evaporator. The residue was dissolved in Et₂O (100 mL) and counter-currently extracted (2 × 2) with 20% aqueous NMe₄Cl. The ethereal phases were combined and rotary evaporated to dryness. The residue was triturated with Et₂O, and the filtered solvent was evaporated to afford the crude product, which was recrystallized from MeOH/water. Yield: 606 mg (54%). For NMe₄⁺ salt: ¹H{¹¹B} NMR δ 3.44 [s, 12H, NMe₄⁺], 1.55 [s, 5H, BH(2-6)], 1.12 [m, 21H, (*i*-Pr₃Si)], -0.16 [s, 5H, CH₃(7-11)], -0.51 [s, 3H, CH₃(12)]. ¹³C{¹H} NMR δ 56.10 [s, N(CH₃)₄⁺], 46.65 [s, C(cage)], 20.44 [s, *i*-Pr CH₃], 14.13 [s, *i*-Pr CH], -1.12 [s, B-CH₃(7-11)], -1.68 [s, B-CH₃(12)]. ¹¹B NMR δ 4.93 [s, B(12)], -4.70 [s, 5B, B(7-11)], -15.82 [d, 5B, 140, B(2-6)]. IR (KBr) 2930, 2895, 2859, 2533, 1480, 1295, 1122, 1040, 937, 877, 785, 644 cm⁻¹. ESI MS(-) *m/z* 383, expected isotopic distribution. For PPh₄⁺ salt: Anal. Calcd for C₄₀H₆₆B₁₁PSi: C, 66.46; H, 8.92. Found: C, 66.17; H, 8.86.

Tetramethylammonium 7,8,9,10,11-Pentaiodo-12-methylcarba-closo-dodecaborate, [Me₄N][(7-11)-I₅-12-CH₃CB₁₁H₆] (30a): ICl (5.0 g, 3.78 mmol) was added to a solution of Me₄N⁺5a (0.54 g, 2.4 mmol) in dimethoxyethane (20 mL). The mixture was stirred overnight at 65 °C. It was cooled to 0 °C and quenched by adding dropwise a saturated solution of sodium sulfite. After the solvent was removed on a rotary evaporator, the solid was washed with water and recrystallized from water/methanol. Yield: 1.93 g (92%). For PPh₄⁺ salt: ¹H{¹¹B} NMR δ 7.93 [t, 4H, PPh₄⁺], 7.80 [m, 8H, PPh₄⁺], 7.62 [m, 8H, PPh₄⁺], 2.82 [s, 5H, BH(2-6)], 2.51 [s, 1H, CH(1)], 0.10 [s, 3H, CH₃], ¹³C{¹H} NMR δ 136.23 [d, PPh₄⁺], 134.56 [d, PPh₄⁺], 131.24 [d, PPh₄⁺], 52.65 [s, C(1)], 23.24 [s, Ph₃P⁺C], 8.95 [s, CH₃]. ¹¹B NMR (CDCl₃) δ 0.26 [s, 1B, B(12)], -16.10 [d, 5B, B(2-6)], -20.21 [s, 5B, B(7-11)]. IR (KBr pellet) 3433, 3132, 3038, 2591, 1635, 1475, 1302, 972, 844, 697, 611 cm⁻¹. ESI MS(-) *m/z* 787, expected isotopic distribution. Anal. Calcd for C₂₆H₂₉B₁₁PI₅: C, 27.74; H, 2.60. Found: C, 27.50; H, 2.55.

Cesium 1-Triisopropylsilyl-7,8,9,10,11-pentamethyl-12-iodocarbocloso-dodecaborate, [Cs][1-(*i*-Pr₃Si)-(7-11)-Me₅-12-ICB₁₁H₅] (31a): Cs⁺25a (1.16 g, 2.1 mmol) was dissolved in sulfolane (15 mL), then CaH₂ (8.10 g, 0.1 mol) was added. The solution was stirred for 1 h. Methyl triflate (3.5 mL) was added, and the reaction was stirred for 3 d at room temperature. The reaction was monitored by ESI MS. Long reaction times (over 3 d) led to overmethylated product, and stopping

the reaction short (less than 3 d) led to incomplete conversion. The reaction mixture was diluted with diethyl ether (50 mL) and filtered. The filtered white solid (CaH₂) was washed with ether (3 × 50 mL). The ether was washed three times with a 10% aqueous solution of CsCl and removed on a rotary evaporator, and an off-white solid was dried under reduced pressure at 150 °C overnight. The product was recrystallized from water/methanol (90/10) to yield off-white crystals of Cs⁺31a. Yield: 1.03 g (79%). For PPh₄⁺ salt: ¹H{¹¹B} NMR δ 7.92 [t, 4H, PPh₄⁺], 7.78 [m, 8H, PPh₄⁺], 7.61 [m, 8H, PPh₄⁺], 1.66 [s, 5H, BH(2-6)], 1.10 [s, 15H, BCH₃], -0.023 [m, 21H, (*i*-Pr₃Si)]. ¹³C{¹H} NMR δ 135.91 [d, PPh₄⁺], 134.30 [d, PPh₄⁺], 130.79 [d, PPh₄⁺], 117.30 [d, PPh₄⁺], 47.53 [s, C(1)], 19.79 [s, CH₃(*i*-Pr)], 13.35 [s, CH(*i*-Pr)], 13.30 [s, BCH₃]. ¹¹B NMR δ -6.05 [s, 6B, B(7-12)], -17.52 [d, 5B, B(2-6)]. ²⁹Si NMR δ 1.11 [s, *i*-Pr₃Si]. IR (KBr pellet) 3427, 2932, 2890, 2858, 2565, 2517, 2357, 1596, 1437, 1304, 1107, 995, 809, 723, 690, 522 cm⁻¹. MS ESI(-) *m/z* 496, expected isotopic distribution. Anal. Calcd for C₃₉H₆₁B₁₁SiPI: C, 56.11; H, 7.36. Found: C, 55.87; H, 7.12.

Cesium 1,2,3,4,5,6,12-Heptamethyl-7,8,9,10,11-pentaiodocarbocloso-dodecaborate, [Cs][(1-6),12-Me₇-(7-11)-I₅CB₁₁] (32a): *n*-BuLi (1.8 mL, 1.6 M) was added dropwise to a solution of Me₃NH⁺21a (1.06 g, 1.16 mmol) dissolved in THF (30 mL) at 0 °C. The reaction mixture was stirred for 30 min and allowed to reach room temperature. The reaction mixture was again cooled to 0 °C, and CH₃I (0.56 mL) was added dropwise. The mixture was stirred for 2 h and then checked by NMR. The reaction was quenched with methanol (10 mL) followed by an 10% aqueous NaOH solution (20 mL). The volatiles were removed with a rotary evaporator, and CsCl was added to form a white precipitate. Yield: 1.16 g (98%). For PPh₄⁺ salt: ¹H{¹¹B} NMR δ 7.93 [t, 4H, PPh₄⁺], 7.80 [m, 8H, PPh₄⁺], 7.63 [m, 8H, PPh₄⁺], 1.05 [s, 3H, CH₃(1)], 0.14 [s, 15H, CH₃(2-6)], 0.12 [s, 3H, CH₃(12)]. ¹H-¹³C{¹H} gHMBC δ 134.59 [s, PPh₄⁺], 131.44 [s, PPh₄⁺], 16.89 [s, C, CH₃(1)], 2.28 [s, CH₃(2-6,12)]. ¹H{¹³C}{¹¹B} gHMBC δ 58.35 [s, C(1)], ¹¹B NMR δ -2.52 [s, 1B, B(12)], -9.20 [s, 5B, B(2-6)], -17.54 [s, 1B, B(7-11)]. IR (KBr pellet) 3425, 2936, 2895, 1643, 1455, 1394, 1313, 1056, 860 cm⁻¹. ESI MS(-) *m/z* 871, expected isotopic distribution. For PPh₄⁺ salt: Anal. Calcd for C₃₂H₄₁B₁₁PI₅: C, 31.76; H, 3.41. Found: C, 31.84; H, 3.63.

Cesium 1,7,8,9,10,11,12-Heptamethyl-2,3,4,5,6-pentaiodocarbocloso-dodecaborate, [Cs][1,(7-12)-Me₇-(2-6)-I₅CB₁₁] (33a): Cs⁺27a (0.10 g, 0.10 mmol) was dissolved in freshly distilled Et₂O (20 mL) in a three-neck round-bottom flask equipped with a PTFE-clad stir bar and cooled to -78 °C. *n*-BuLi, 1.6 M in hexanes (0.25 mL, 0.40 mmol), was added dropwise over 1 h using a syringe pump, and stirring was continued for an additional 1 h. Methyl iodide (60 mg, 0.40 mmol) was added, and the mixture was stirred for an additional 30 min. Water (20 mL) was added, and the solvents were removed on a rotary evaporator. The remaining solids were triturated with Et₂O (3 × 50 mL), and the combined Et₂O solutions were washed with a 20% aqueous CsCl solution (3 × 50 mL). The combined CsCl wash was extracted with Et₂O (3 × 50 mL), and all ethereal solutions were pooled and evaporated on a rotary evaporator. The remaining solid was triturated with Et₂O and filtered. The Et₂O was evaporated, and the solid was recrystallized from acetone/water providing Cs⁺33a. Yield 91 mg (90%). For Cs⁺ salt: ¹H{¹¹B} NMR δ -0.25 [s, 3H, BCH₃(12)], -0.05 [s, 15H, BCH₃(7-11)], 2.00 [s, 3H, CH₃(1)]. ¹H{¹³C}{¹¹B} gHMBC δ -0.01 [s, BCH₃(12)], 2.20 [s, BCH₃(7-11)], 28.50 [s, CH₃(1)]. ¹H-¹³C{¹¹B} gHMBC δ 45.20 (s, cage). ¹¹B{¹H} NMR: δ -17.45 [s, 5B, B(2-6)], -4.887 [s, 5B, B(7-11)], 0.48 [s, 1B, B(12)]. IR (KBr) 2945, 2800, 2776, 1480, 1300, 1112, 1010, 870, 735, 520 cm⁻¹. ESI MS(-) *m/z* 871, expected isotopic distribution. For PPh₄⁺ salt: Anal. Calcd for C₃₂H₄₁I₅B₁₁P: C, 31.76; H, 3.42. Found: C, 31.91; H, 3.37.

Tetraphenylphosphonium 12-Iodo-2,3,4,5,6,7,8,9,10,11-decamethylcarba-closo-dodecaborate, [Ph₄P][(12-I-(2-11)-Me₁₀CB₁₁H)] (36a): Me₄N⁺20a (1.00 g, 2.9 mmol) was methylated according to the procedure described for 16a, providing a white solid after recrystalli-

zation from methanol. Yield: 1.68 g (77%). For Cs⁺ salt: ¹H NMR δ 1.37 [s, 1H, CH(1)], -0.11 [s, 15H, CH₃(2-6)], -0.22 [s, 15H, CH₃(7-11)]. For Ph₄P⁺ salt: ¹³C{¹H, ¹¹B(selective)} NMR δ -1.75 [CH₃(2-6)], -0.93 [s, CH₃(7-11)], 62.31 [s, C(1)], 118.84 [d, PPh₄⁺], 131.26 [d, PPh₄⁺], 135.56 [d, PPh₄⁺], 136.28 [d, PPh₄⁺]. ¹¹B NMR δ -5.51 [s, 1B, B(12)], -9.11 [s, 5B, (7-11)], -12.26 [s, 5B, (2-6)]. For Cs⁺ salt: IR (KBr pellet) 2928, 2895, 2829, 2530, 2447, 2360, 1457, 1306, 1038 cm⁻¹. ESI MS (-) *m/z* 409, expected isotopic distribution. For PPh₄⁺ salt: Anal. Calcd for C₃₅B₁₁H₅₁PI: C, 56.16; H, 6.87. Found: C, 56.19; H, 7.01.

Tetraphenylphosphonium 12-Iodo-1,2,3,4,5,6,7,8,9,10,11-undecamethylcarba-closo-dodecaborate, [Ph₄P][12-I-(1-11)-Me₁₁CB₁₁] (37a). Me₄N⁺23a (1.00 g, 4.1 mmol) was methylated according to the procedure described for 16a, providing a white solid after recrystallization from methanol. Yield: 1.19 g (56%). For Cs⁺ salt: ¹H NMR δ 0.80 [s, 3H, CH₃(1)], -0.21 [s, 15H, CH₃(2-6)], -0.26 [s, 15H, CH₃(7-11)]. For Ph₄P⁺ salt: ¹³C{¹H, ¹¹B(selective)} NMR δ -3.18 [CH₃(2-6)], -0.86 [s, CH₃(7-11)], 13.14 [s, CH₃(1)], 58.39 [s, C(1)], 118.92 [d, PPh₄⁺], 131.32 [d, PPh₄⁺], 135.62 [d, PPh₄⁺], 136.32 [d, PPh₄⁺]. ¹¹B NMR δ -5.60 [s, 1B, B(12)], -9.16 [s, 5B, (7-11)], -10.98 [s, 5B, (2-6)]. For Cs⁺ salt: IR (KBr pellet) 2920, 2897, 2824, 1607, 1424, 1370, 1309, 1149, 920, 809 cm⁻¹. ESI MS (-) *m/z* 423, expected isotopic distribution. For PPh₄⁺ salt: Anal. Calcd for C₃₆H₅₃B₁₁PI: C, 56.70; H, 7.00. Found: C, 56.40; H, 7.07.

Cesium 1-Hexylcarba-closo-dodecaborate, [Cs][1-hexyl-CB₁₁H₁₁] (38a): Cs⁺1a (1.0 g, 4.9 mmol) was dissolved in freshly distilled THF (100 mL) in a three-neck round-bottom flask equipped with a PTFE-clad stir bar and cooled to 0 °C. *n*-BuLi, 1.6 M in hexanes (12.25 mL, 19.6 mmol), was added via a syringe pump over 1 h. The reaction mixture was stirred for an additional 1 h, and then 1-bromohexane (2.75 mL, 19.6 mmol) was added. The reaction mixture was stirred for an additional 30 min at which time water (50 mL) was added, and the solvents were removed on a rotary evaporator. The resulting solids were washed with Et₂O (3 × 50 mL). The combined ethereal solution was partitioned with a 20% aqueous solution of CsCl (3 × 50 mL). The CsCl solution was then washed with Et₂O (3 × 50 mL). The combined ethereal solutions were evaporated to dryness, the remaining solids were triturated with Et₂O, and the filtered organic solution was evaporated to dryness to provide Cs⁺38a. Yield, 1.66 g (94%). For Cs⁺ salt: ¹H-¹¹B NMR δ 0.84 (t, 3H, CH₃), 1.11 (m, 2H, CH₂), 1.28 [m, 6H, (CH₂)₃], 1.56 [s, 5H, BH(7-11)], 1.64 [s, 1H, BH(12)], 1.75 [s, 5H, BH(2-6)], 1.76 (t, 2H, CH₂). ¹H{¹³C}{¹¹B} gHMBC δ 13.80 [s, CH₂], 29.50 [s, CH₂], 29.7 [s, CH₂], 30.00 [s, CH₂], 31.50 [s, CH₂], 39.50 [s, CH₃]. ¹H{¹³C}{¹¹B} gHMBC δ 70.50 [s, C(1)]. ¹¹B{¹H} NMR: δ -13.50 [s, 10B, B(2-11)], -9.99 [s, 1B, B(12)]. IR (KBr) 2940, 2872, 2543, 1462, 1312, 1197, 1041, 935, 732, 523 cm⁻¹. ESI MS(-) *m/z* 228, expected isotopic distribution. For PPh₄⁺ salt: Anal. Calcd for C₃₁H₄₄B₁₁P: C, 65.72; H, 7.83. Found: C, 65.63; H, 7.79.

Cesium 1-Hexyl-2,3,4,5,6,7,8,9,10,11,12-undecamethylcarba-closo-dodecaborate, [Cs][1-hexyl-CB₁₁Me₁₁] (39a): Cs⁺38a (1.0 g, 2.8 mmol) was dissolved in sulfolane (15 mL) in a 250 mL, three-neck, round-bottomed flask, and the system was placed under argon. Calcium hydride (4.7 g, 112 mmol) was added, and the solution was stirred for 30 min. Methyl triflate (9.2 g, 56 mmol) was added at 25 °C over a 20 h period via a syringe pump. The stirring was continued for 2 d, after which additional methyl triflate (4.6 g, 28 mmol) was added in one portion. The reaction mixture was stirred for an additional 2-3 d, and the reaction progress was monitored by ESI-MS. Upon reaction completion the mixture was diluted with anhydrous methylene chloride (300 mL) and CaH₂ was removed by vacuum filtration.

The filtrate was quenched with 27% ammonium hydroxide (100 mL), and the methylene chloride was distilled off. The remaining aqueous solution was extracted with Et₂O (3 × 50 mL), and the combined ethereal solution was washed with a 20% aqueous solution of CsCl (3 × 50 mL). The CsCl solution was extracted with Et₂O (3 × 50 mL), and the organic solutions were combined and evaporated to dryness

on a rotary evaporator. The remaining solid was washed with Et₂O (3 × 50 mL), and residual CsCl was filtered off. The ethereal solution was evaporated to dryness, and the remaining solid was dried at 150 °C and 0.05 Torr for 48 h to remove residual sulfolane. The solid was then recrystallized from boiling water. Yield: 1.31 g (71%). For Cs⁺ salt: ¹H{¹¹B} NMR δ -0.51 [s, 3H, BCH₃(12)], -0.41 [s, 15H, BCH₃(7-11)], -0.19 [s, 15H, BCH₃(2-6)], 0.86 (t, 3H, CH₃), 1.08 (m, 2H, CH₂), 1.26 [m, 6H, (CH₂)₃], 1.54 (m, 2H, CH₂). ¹H{¹³C}{¹¹B} gHMBC δ -5.0 [s, BCH₃(12)], -4.0 [s, BCH₃(7-11)], -2.0 [s, BCH₃(2-6)], 14.0 [CH₃], 14.1 [CH₂], 23.0 [s, (CH₂)₂], 31.5 [CH₂], 32.5 [s, CH₂]. ¹H{¹³C}{¹¹B} gHMBC δ 58.5 [C(1)]. ¹¹B NMR: δ -10.51 [s, 5B, B(2-6)], -8.44 [s, 5B, B(7-11)], 0.05 [s, 1B, B(12)]. IR (KBr) 2927, 2895, 2829, 1448, 1412, 1352, 1300, 1254, 1215, 1145, 1033, 908, 735, 571, 440 cm⁻¹. ESI MS(-) *m/z* 381, expected isotopic distribution. For PPh₄⁺ salt: Anal. Calcd for C₄₂H₆₆B₁₁P: C, 69.98; H, 9.23. Found: C, 69.67; H, 9.14.

Tetramethylammonium 1-Triisopropylsilyl-7,8,9,10,11,12-hexaethylcarba-closo-dodecaborate, [NMe₄][1-(*i*-Pr₃Si)-(7-12)-Et₆CB₁₁H₅] (40a): Cs⁺18a (1.00 g, 2.32 mmol) was combined with CaH₂ (10.0 g, 250 mmol) and sulfolane (50 mL) in a round-bottom flask (250 mL) equipped with a stir bar. Freshly prepared EtOTf (10 mL, 63 mmol) was added using a syringe pump over 18 h. The reaction was constantly monitored with ESI/MS to prevent overethylation. After 3 d at rt, the mixture was diluted with CH₂Cl₂ (200 mL) and filtered through a coarse frit. The filtrate was quenched with saturated NH₃OH (40 mL) and then evaporated to dryness using a rotary evaporator. The residue was dissolved in Et₂O (100 mL) and countercurrent extracted (2 × 2) with 20% aqueous NMe₄Cl. The ethereal phases were combined and rotary evaporated to dryness. The residue was triturated with Et₂O, and the filtered solvent was evaporated to afford the crude product, which was recrystallized from MeOH/water. Yield: 870 mg (63%). For NMe₄⁺ salt: ¹H{¹¹B} NMR δ 3.39 [s, 12H, N(CH₃)₄⁺], 1.12 [m, 21H, (*i*-Pr₃-Si)], 1.63 [s, 5H, BH(2-6)], 0.99 [br, BCH₃(7-12)], 0.50 [br, BCH₂(7-12)]. ¹³C{¹H} NMR δ 55.7 [s, N(CH₃)₄⁺], 50.02 [s, C(1)], 20.88 [s, *i*-PrCH₃], 14.50 [s, *i*-PrCH], 10.88 [br, BCH₃(7-12)], 6.32 [br, BCH₂(7-12)]. ¹¹B NMR δ 4.08 [s, 1B, B(12)], -3.32 [s, 5B, B(7-11)], -16.42 [d, 5B, B(2-6)]. IR (KBr) 2995, 2872, 2820, 2555, 1501, 1286, 1164, 1058, 943, 888, 765, 640 cm⁻¹. ESI MS(-) *m/z* 469, expected isotopic distribution. For PPh₄⁺ salt: Anal. Calcd for C₄₆H₇₆B₁₁PSi: C, 68.46; H, 9.49. Found: C, 68.90; H, 9.89.

Cesium 7,8,9,10,11,12-Hexaethylcarba-closo-dodecaborate, [Cs][[(7-12)-Et₆CB₁₁H₆] (41a): Cs⁺40a (500 mg, 0.87 mmol) was dissolved in sulfolane (30 mL) in a round-bottom flask equipped with a reflux condenser, and the system was put under an Ar atmosphere. CsF (270 mg) was added, and the reaction mixture was heated to 225 °C using a Wood's metal bath. After 4 h, additional CsF (2.0 g) was added and the reaction mixture heated to 270 °C. After an additional 3 h, more CsF (500 mg) was added and the reaction mixture was heated an additional 12 h at 270 °C. The reaction mixture was poured into water (100 mL) and extracted with Et₂O (2 × 50 mL). The combined ether layers were partitioned against a 20% aqueous CsCl solution (50 mL, countercurrent, 2 × 2). The ethereal phase was evaporated to dryness, and the resulting solid was triturated with Et₂O. The filtered ether was evaporated to dryness, and the residue was recrystallized from hot water. Yield: 320 mg (83%). For Cs⁺ salt: ¹H{¹¹B} NMR δ 1.95 [s, 1H, CH(1)], 1.22 [s, 5H, BH(2-6)], 0.48 [br s, 18H, BCH₃], 0.11 [br s, 12H, BCH₂]. ¹³C{¹¹B} NMR δ 42.14 [s, C(1)], 0.74 [s, BCH₂], -1.51 [s, BCH₃(7-11)], -2.32 [s, BCH₃(12)]. ¹¹B NMR δ 2.80 [s, 1B, B(12)], -4.02 [d, 5B, B(7-11)], -18.30 [d, 5B, B(2-6)]. IR (KBr) 2995, 2870, 2815, 2499, 2451, 1282, 1160, 1073, 990, 865 cm⁻¹. ESI MS (-) *m/z* 311, expected isotopic distribution. For PPh₄⁺ salt: Anal. Calcd for C₃₇H₅₆B₁₁P: C, 68.29; H, 8.67. Found: C, 68.32; H, 8.70.

Tetraphenylphosphonium 2,3,4,5,6-Pentaethyl-7,8,9,10,11,12-hexamethylcarba-closo-dodecaborate, [Ph₄P][1-H-(2-6)-Et₅-(7-12)-Me₆CB₁₁] (42a): Cs⁺11a (0.65 g, 1.81 mmol) was combined with CaH₂

(10.0 g, 250 mmol) and sulfolane (50 mL) in a round-bottom flask (250 mL) equipped with a stir bar. EtOTf (10 mL, 63 mmol) was added using a syringe pump over 18 h. After 3 d at rt, the mixture was diluted with CH₂Cl₂ (200 mL) and filtered through a coarse frit. The filtrate was quenched with 27% NH₄OH (40 mL) and then evaporated to dryness using a rotary evaporator. The residue was dissolved in Et₂O (100 mL) and countercurrent extracted (2 × 2) with 20% aqueous CsCl. The ethereal phases were combined and rotary evaporated to dryness. The residue was triturated with Et₂O, and the filtered solvent was evaporated to afford the crude product, which was recrystallized from MeOH/water. Yield: 550 mg (61%). For PPh₄⁺ salt: ¹H{¹¹B} NMR (Ph₄P⁺) δ 8.20 [m, 4H, PPh₄⁺], 7.77 [m, 8H, PPh₄⁺], 7.70 [m, 8H, PPh₄⁺], 1.25 [s, 1H, B(2)], 0.91 [t, 15H, CH₃(7–11)], 0.80 [t, 3H, CH₃-(12)], 0.55 [br s, 15H, BCH₃(2–6)], 0.21 [br s, 10H, BCH₂(2–6)]. ¹³C{¹H} NMR δ -2.01 [s, BCH₃(12)], -1.42 [s, BCH₃(7–11)], 7.24 [s, BCH₂(2–6)], 12.45 [s, BCH₃(2–6)], 45.35 [s, C(1)], 122.24 [d, PPh₄⁺], 131.88 [d, PPh₄⁺], 135.90 [d, PPh₄⁺], 136.39 [d, PPh₄⁺]. ¹¹B NMR δ 1.95 [s, B(12)], -2.24 [s, 5B, B(7–11)], -8.55 [s, 5B, B(2–6)]. IR (KBr) 2980, 2865, 2812, 2533, 1490, 1277, 1152, 1025, 922,

866, 760, 624 cm⁻¹. ESI MS (-) *m/z* 369, expected isotopic distribution. Anal. Calcd for C₄₁H₆₄B₁₁P: C, 69.67; H, 9.13. Found: C, 69.60; H, 9.05.

Acknowledgment. We are grateful to Dr. Joshua R. Smith for assistance. This work was supported by the U.S. NSF (CHE-0446688 and OISE-0532040) and the Czech MŠMT (program KONTAKT, Project ME 857).

Supporting Information Available: Complete ref 62, a computer program nao2cluster for a conversion of the valence part of an MO from a natural atomic orbital basis into an icosahedral cluster basis (C program source code in .txt format; rename to .c after downloading), and a table of energies obtained in RI-DFT(B-P)/TZVP calculations. This material is available free of charge via the Internet at <http://pubs.acs.org>.

JA066247Z